Computational Studies of Photophysical and Aromatic Properties of Porphyrinoids and Acenes

Isaac Benkyi

University of Helsinki
Faculty of Science
Department of Chemistry
A. I. Virtasen aukio 1 (P. O. Box 55)
FI-00014 University of Helsinki, Finland

To be presented for public examination with the permission of the Faculty of Science of the University of Helsinki, Auditorium A 129 Chemistry (A. I Virtasen aukio 1), on June 17, 2022 at 12 o'clock

Helsinki 2022

Supervised by:
Prof. Dage Sundholm
University of Helsinki
Department of Chemistry
Finland

Reviewed by:
Prof. Christel Marian
University of Düsseldorf
Institute of Theoretical and Computational Chemistry
Germany

Privatdozent Dr. Raphael J. F. Berger
University of Salzburg
Chemistry of Materials
Austria

Opponent:
Dr. Michael Patzschke
Helmholtz-Zentrum Dresden-Rossendorf
Department of Chemistry
Germany

Custos:
Prof. Dage Sundholm
University of Helsinki
Department of Chemistry
Finland

ISBN 978-951-51-8244-9 (paperback)
ISBN 978-951-51-8245-6 (PDF)
Unigrafia
Helsinki 2022

Abstract

Expanded porphyrins, porphyrinoids, porphycenes and N-doped nanographenes are multi-ring molecules whose aromaticity cannot be easily predicted based on NMR chemical shifts. The magnetically induced current-density susceptibility and the ring-current pathways have been elucidated for these molecules at *ab initio* and density functional theory (DFT) levels using the gauge including magnetically induced current (GIMIC) method. Calculations showed that the lowest electronic transition of the antiaromatic molecules are purely magnetic transitions which is also the main reason why these molecules sustain large net paratropic ring currents.

The photophysical properties of expanded porphyrins, acenes and pyrene have also been studied using quantum mechanical methods. The absorption spectrum including vibrational bands of the acenes and pyrene were simulated and compared with those obtained in high-resolution measurements of the absorption spectra in the visible range. The vibrational contributions to the absorption spectra were obtained by using a time-generating function approach, which is computationally faster than alternative approaches. The 0-0 transition energies of acenes and pyrene are reported. Various vibrational modes contributing to the vibrational fine structure of these molecules have been identified. The quantum yield of luminescence was determined for the expanded porphyrins by calculating rate constants for radiative and non-radiative transitions between excited electronic states and the ground state.

Acknowledgement

This work could not have been completed without the support and assistance of several individuals who contributed in diverse ways.

I would like to express my heartfelt gratitude to my supervisor Dage Sundholm. You are one of the few warm-hearted people I have encountered in my educational endeavour. Words can not express how grateful I am to you.

I am also indebted to my co-authors especially Enrico Tapavicza, who provided me the code for my third article, and Heike Fliegl who gave me a head start to the GIMIC method.

To my colleagues in the Sundholm group, you created a great environment for me to be able to complete this work. I am much grateful for your company.

I want to thank the Swedish Cultural Foundation in Finland, and the Academy of Finland for funding this work. I also thank the Doctoral Programme in Chemistry and Molecular Science (CHEMS) for funding my conference attendance.

My family and friends, those abroad and in Finland, I really appreciate your support and encouragement throughout the journey.

List of Publications

This thesis is based on the following publications.

I Valiev, R. R., Benkyi, I., Konyshev, Y. V., Fliegl, H. & Sundholm, D. *Computational studies of aromatic and photophysical properties of expanded porphyrins.* J. Phys. Chem. A, 122(20), 4756–4767. doi:10.1021/acs.jpca.8b02311 **(2018)**.

II Benkyi, I. & Sundholm, D. *Aromatic pathways in porphycene derivatives based on current-density calculations.* J. Phys. Chem. A, 123(1), 284–292. doi:10.1021/acs.jpca.8b10818 **(2018)**.

III Benkyi, I., Tapavicza, E., Fliegl, H., & Sundholm, D. *Calculation of vibrationally resolved absorption spectra of acenes and pyrene.* Phys. Chem. Chem. Phys. 21(37), 21094–21103. doi:10.1039/C9CP04178H **(2019)**.

IV Benkyi, I., Staszewska-Krajewska, O., Gryko, D. T., Jaszunski, M., Stanger, A., & Sundholm, D. *The interplay of aromaticity and antiaromaticity in N-doped nanographenes*. J. Phys. Chem. A, 124(4), 695–703. doi:10.1021acs.jpca.9b11315 **(2020)**.

The candidate, Isaac Benkyi (IB), performed the current density calculations for all the molecules at the Hartree-Fock and MP2 levels of theory as well as the DFT level using different functionals for Article I. IB also participated in the preparation of the manuscript. All the calculations for Article II & III were performed by IB. The manuscripts were prepared by IB. For Article IV, IB calculated and elucidated the ring-current susceptibility and pathways for the GIMIC section. IB also contributed to the preparation of the manuscript.

Contents

1 Introduction

The interaction of light with molecules can result in transfer of the photon energy to the electrons of the molecules. The light absorption leads to an excitation of electrons in the molecule to a higher energy state. Since each electronic state has its own unique vibrational energy levels, this results in a fine structure of the absorption band. At ambient conditions, the excitation from the ground energy state occurs from the lowest vibrational energy level. The transition probability from the lower energy state to a vibrational energy level of the higher electronic energy state depends to first order on the shape of the potential energy surface of the excited state and the overlap of the vibrational wavefunction of the two states. Experimentally, this is observed as a fine structure in high-resolution electronic absorption spectra.

Nowadays, simulating absorption spectra of molecules including fine details, such as the coupling between the nuclear and electronic degrees of freedom, and changes in the molecular structure of excited states is an active field of research.[1–6] These studies comprise computing vertical excitation energies combined with molecular dynamics (MD) simulations, computing vertical excitation energies and combining them with the calculations of individual Franck-Condon factors between the involved vibrational levels.[1,7–10]

The development of time-dependent density functional theory (TDDFT) methods has provided a powerful tool, which chemists can use in calculating vertical excitation energies of molecules. This approach can be used for estimating the band maximum of the absorption spectrum, which provides a first estimate for the energy of the electronic transition.[11–14] Even though this approach yields a crude approximation, it is often used because it is computationally cheaper than more accurate approaches. However, fine details about the vibrational structure of the molecule, which can be deduced from the recorded spectrum are lost. In this thesis, absorption spectra of the molecules have been simulated using the RADLESS module of the TURBOMOLE program package.[4,15] The RADLESS module calculates the vibrational contributions to the absorption band using a time-generating function instead of computing individual Franck-Condon factors.

Aromaticity is one of the most vague concepts in chemistry. Since the discovery of benzene by Kekulé,[16] chemists have been intrigued by the concept. Aromaticity is currently an active research area.[17–20] Understanding molecular aromaticity provides useful information about the electronic structure of the molecule and the electron delocalization pathways.[21–23] Several criteria are used for defining the extent of molecular aromaticity.[24–30] One of the often used method to determine the degree of aromaticity is based on the strength of the ring current, which is determined indirectly by calculating magnetic shielding constants or by measuring NMR chemical shifts. The gauge including magnetically induced current (GIMIC) approach used in this thesis is based on a ring-current integration approach. The GIMIC approach has been widely used to determine the aromatic or antiaromatic character of varieties of molecule.[31–34]

This thesis is organized as follows. Chapter 2 provides a brief overview of the electronic structure theory methods used in the thesis. Chapter 3 focuses on the theory of magnetically induced current densities in molecules and the theoretical framework of the GIMIC method. Chapter 4 elaborates on some photophysical properties of molecules.

The obtained results are summarized in chapter 5 and concluding remarks are given in Chapter 6.

2 Electronic Structure Theory

In this section, the theory of electronic structure methods, which were used in this thesis is briefly reviewed.

2.1 Schrödinger Equation

The Schrödinger equation is the fundamental equation for describing the quantum mechanical behaviour of particles.[35] It is a first order differential equation with respect to time (t).

$$i\hbar\frac{\partial\Psi(r,t)}{\partial t} = \hat{H}\Psi(r,t) \tag{2.1}$$

where r represents the Cartesian x, y and z coordinates, Ψ is the time-dependent wave function, and $\hat{H}$ is the Hamiltonian. Equation 2.1 is the time-dependent Schrödinger equation. The time-independent equation is an eigenvalue equation and is written as

$$\hat{H}\psi = E\psi \tag{2.2}$$

where E is the energy eigenvalue and, ψ, the time-independent wave function is the eigen solution of the eigenvalue equation. The wave function contains all information we may need about our system.

The Hamiltonian operator is the sum of the potential $\hat{V}$ and kinetic $\hat{T}$ energy operators.

$$\hat{H} = \hat{T} + \hat{V} \tag{2.3}$$

The kinetic energy operator is given by

$$\hat{T} = -\Big(\frac{\hbar}{2m}\Big)\nabla^2 \tag{2.4}$$

where $\hbar$ is the Dirac constant, m is the mass of the particle, and ∇^2 is the Laplace operator that is given in Cartesian coordinates as

$$\nabla^2 = \frac{\partial^2}{\partial x^2} + \frac{\partial^2}{\partial y^2} + \frac{\partial^2}{\partial z^2} \tag{2.5}$$

For a system of n-electrons and and N-nuclei, the total Hamiltonian is the sum of the kinetic energy terms of the electrons (T_e) and nuclei (T_N) and the potential (V) energy term representing the interaction between the particles of the system .

$$H = T_e + T_N + V \tag{2.6}$$

For simplicity, the Hartree atomic unit for energy (a.u) is used in the rest of this chapter. The atomic units are defined by setting the charge of the electron, e, its mass m_e, the Dirac

constant $\hbar$, and the Bohr radius a_0 to unity. The total Hamiltonian can then be written as

$$H = -\sum_{i=1}^{n} \frac{1}{2}\nabla_i^2 - \sum_{A=1}^{N} \frac{1}{2M_A}\nabla_A^2 - \sum_{i,A} \frac{Z_A}{r_{iA}} + \sum_{i>j} \frac{1}{r_{ij}} + \sum_{B>A} \frac{Z_A Z_B}{R_{AB}} \tag{2.7}$$

where M_A is the mass of the nuclei; Z_A and Z_B are the nuclei charge; R_{AB} is the internuclear distance; r_{iA} is the electron-nuclear distances, and r_{ij} is the electron-electron distance. Analytical solutions for Equation 2.6 exist only for systems with one electron such as the hydrogen atom. Going beyond a single electron problem, the equation becomes analytically unsolvable. In order to solve the Schrödinger equation for systems with more than one electron, several approximations are introduced.

The Born-Oppenheimer approximation is based on the fact that the nuclei are much heavier than the electrons and thus the electrons can respond almost instantaneously to displacements of the nuclei.[36] Hence, by keeping the nuclei fixed we can solve the Schrödinger equation of the electrons. Applying this approximation, the electronic Hamiltonian of the Schrödinger equation to be solved is

$$\hat{H} = -\sum_{i=1}^{n} \frac{1}{2}\nabla_i^2 - \sum_{i,A} \frac{Z_A}{r_{iA}} + \sum_{i>j} \frac{1}{r_{ij}} + \sum_{B>A} \frac{Z_A Z_B}{R_{AB}} \tag{2.8}$$

The Born-Oppenheimer approximation assumes that the nuclear kinetic energy term can be ignored, while the electronic interactions depend parametrically on the nuclei positions. However, it is a well-known fact that the vibrational and electronic interaction are interrelated.[37] This is referred to as vibronic coupling, which has to be considered in non-adiabatic processes.[38]

2.2 Hartree-Fock Approximation

In the Hartree-Fock (HF) approximation,[39,40] one looks for approximate one-electron wave function for the Schrödinger equation. It is assumed that the electrons do not interact instantaneously with with each other, the interaction is rather treated as a mean field created by the other electrons. The wave function can then be approximated as product of the one-electron wave functions which is the called the Hartree product.

$$\psi(r_1, r_2, ..., r_N) = \phi_1(r_1)\phi_2(r_2)...\phi_N(r_N) \tag{2.9}$$

The electrons possess an intrinsic angular momentum, namely the up or down spin. Thus the electronic wave function must also include the spin, which can adopt two values, often called α or β, in addition to the spatial wave function. The spin orbital (χ) is written as a product of the spatial orbital (ϕ) and the spin function.

Equation 2.9 does not satisfy the antisymmetry principle, which requires that the wave function describing fermions must be antisymmetric under the exchange of any two electrons. The antisymmetry principle is fulfilled by writing the many-electron wave function

as a Slater determinant.

$$\Psi = \frac{1}{\sqrt{(N!)}} \begin{vmatrix} \chi_1(r_1) & \chi_2(r_1) & \cdots & \chi_N(r_1) \\ \chi_1(r_2) & \chi_2(r_2) & \cdots & \chi_N(r_2) \\ \vdots & \vdots & \cdots & \vdots \\ \chi_1(r_N) & \chi_2(r_N) & \cdots & \chi_N(r_N) \end{vmatrix} \tag{2.10}$$

The Hartree-Fock energy can then be expressed as

$$E_{HF} = \langle \Psi_{HF} | \hat{H} | \Psi_{HF} \rangle = \sum_{i}^{n} h_i + \frac{1}{2} \sum_{i=1}^{n} \sum_{j=1}^{n} (J_{ij} - K_{ij}) \tag{2.11}$$

where n is the number of electrons; V_{NN} is the nuclei-nuclei potential; h_i is given by

$$h_i = \int \psi_i^* \Big[-\frac{1}{2} \nabla_i^2 - \sum_{A}^{N} \frac{Z_A}{|R_A - r_i|} \Big] \psi_i \mathrm{d}v \tag{2.12}$$

where N is the number of nuclei. J_{ij} and K_{ij} in Equation 2.11 are referred to as the Coulomb and exchange integrals, respectively.

$$J_{ij} = \int \psi_i^*(1) \psi_j^*(2) \left(\frac{1}{r_{12}} \right) \psi_i(1) \psi_j(2) \mathrm{d}v_1 \mathrm{d}v_2 \tag{2.13}$$

The Coulomb term accounts for the average repulsion between two electrons

$$K_{ij} = \int \psi_i^*(1) \psi_j^*(2) \left(\frac{1}{r_{12}} \right) \psi_i(2) \psi_j(1) dv_1 dv_2 \tag{2.14}$$

The exchange term describes the interaction due to the interchange of electrons.

Solving equation 2.11 is a difficult task, as one has to evaluate the value of the orbitals at every single point in space. Roothaan suggested that the one-electron wave functions are expanded as a linear combination of atomic orbitals (LCAO), where ϕ_k forms the basis set.[41]

$$\psi_i = \sum_{k}^{n} c_{ki} \phi_k \tag{2.15}$$

The Hartree-Fock equation can then be formulated as a matrix equation, called the Hartree-Fock-Roothaan equation which is given by

$$Fc = Sc\epsilon_i \tag{2.16}$$

where F is the Fock matrix, c is a matrix containing the molecular orbital coefficients, S is the overlap matrix of the basis functions, and ϵ_i are the orbital energies.

The Hartree-Fock method is sometimes referred to as the self-consistent field method because it is a non-linear equation that is solved iteratively until convergence criteria are satisfied for the orbitals and the energy.[42] Since the electrons interact instantaneously

with each other, the assumption made in the derivation of the Hartree-Fock method that electrons interact with the mean-field potential created by the other electrons is a severe approximation. The difference between the mean-field approximation and the instantaneous interactions is referred to as electron correlation.

2.3 Post Hartree-Fock Methods

The main limitations of the Hartree-Fock (HF) method can be avoided by using a multi-determinant wave function ansatz. Methods that incorporate electron correlation effects are called post Hartree-Fock methods.

2.3.1 Configuration Interaction

In the configuration interaction (CI) method, the wave function is expressed as a linear combination of Slater determinant. By using the Hartree-Fock determinant as a starting point, a linear expansion of the determinant is formed by exciting electrons from occupied orbitals to the virtual space. The CI wave function is expressed as a linear combination of the many-body state functions.

$$\Psi_{CI} = \sum_{i=0} c_i \phi_i = c_0\phi_0 + c_1\phi_1 + c_2\phi_2 + \cdots \tag{2.17}$$

The first term in Equation 2.17 is generally the Hartree-Fock determinant. The higher-order terms are configurations that are obtained by formally 'exciting' electrons to the virtual space. When all electrons are 'excited', the model is called full configuration interaction (FCI), which is the exact solution of the Schrödinger equation in the employed basis set. The c_i coefficients are obtained variationally by diagonalizing the Hamiltonian matrix of the configuration space. However, for most practical purposes, this is computationally too expensive. Thus, the expansion in configuration state functions must be truncated. When the construction of the configuration state functions are truncated to singles, doubles and triples 'excitations', configuration interaction singles (CIS), configuration interaction singles and doubles (CISD) and configuration interaction singles, doubles and triples (CISDT) models are obtained, respectively. Truncated CI methods are size-inconsistent, implying the energy when two particles are separated infinitely apart is not exactly twice that of the energy of the single particle.

2.3.2 Coupled-Cluster

The coupled-cluster approach is in principle similar to the configuration interaction method. However, in coupled-cluster methods an exponential cluster operator is used when 'exciting' electrons from the occupied orbitals to virtual ones. The coupled cluster wave function is expressed as

$$|\Psi\rangle = e^{\hat{T}}|\phi_0\rangle \tag{2.18}$$

where ϕ_0 is the reference wave function, which in most cases is the Hartree-Fock Slater determinant. $\hat{T}$ is the excitation operator which acts on the reference wave function to generate correlating Slater determinants by applying single, double etc. excitations. The coupled-cluster energy is expressed using a similarity transformed Hamiltonian as

$$\langle\phi_0|e^{-T}He^{T}|\phi_0\rangle = E\langle\phi_0|\phi_0\rangle \tag{2.19}$$

The exponential operator $e^{\hat{T}}$ is expanded as a Taylor-series

$$e^{\hat{T}} = \sum_{j=0}^{\infty}\frac{\hat{T}^j}{j!} = 1 + \hat{T} + \frac{\hat{T}^2}{2!} + \cdots \tag{2.20}$$

The cluster operator $\hat{T}$ is written as a sum of different excitation orders as

$$\hat{T} = \hat{T}_1 + \hat{T}_2 + \cdots + \hat{T}_N \tag{2.21}$$

where $\hat{T}_1$ is the operator considering single excitations, $\hat{T}_2$, is the operator for double excitations, etc. The cluster operator for single excitations $\hat{T}_1$ is given by

$$\hat{T}_1\phi_0 = \sum_{a=1}^{N}\sum_{i=1}^{n} t_i^a\phi_i^a \tag{2.22}$$

where n is the number of occupied spin orbitals; N is the number of virtual orbitals; and ϕ_i^a is the singly excited Slater determinant in which an occupied orbital i is replaced with a virtual orbital a; t_i^a is a coefficient called the *cluster amplitude*. Similarly, the cluster operator for two electron excitations is

$$\hat{T}_2\phi_0 = \sum_{j>i}^{N}\sum_{b>a}^{n} t_{ij}^{ab}\phi_{ij}^{ab} \tag{2.23}$$

ϕ_{ij}^{ab} is the Slater determinant obtained when the occupied orbitals i and j are replaced by virtual orbitals a and b, and t_{ij}^{ab} is the cluster amplitude. The excitation operator T is generally truncated to lower order excitations such as in the coupled-cluster singles and doubles (CCSD) level. Coupled-cluster singles, doubles and triples (CCSDT) which includes also triple excitations gives very accurate correlation energies but are computationally expensive.

The second-order approximate coupled-cluster singles and doubles model (CC2) is an approximation to CCSD which is often used in calculation of excitation energies.[43] The main difference between the CCSD and CC2 method is that, in CC2 the doubles equations is approximated to the form occurring in first order but the singles are retained to provide an approximate description of orbital relaxation. The quality of the ground-state total energy in the CC2 model is similar to that of Møller-Plesset perturbation theory (MP2). The CC2 model is mainly used in the calculation of excited state energies.

2.3.3 Møller-Plesset Perturbation Theory

The Møller-Plesset perturbation theory considers electron correlation as a perturbation.

$$\hat{H} = \hat{H}_0 + \lambda \hat{V} \tag{2.24}$$

where $\hat{H}_0$ is the unperturbed Hamiltonian, $\hat{V}$ is the perturbation and λ is an arbitrary real parameter that determine the extent and order of the perturbation. The idea of perturbation theory goes back to the work of Schrödinger and Rayleigh, however, the current form of perturbation theory used in electronic structure codes was published in the early 1930s by Møller and Plesset.[44] Their method uses the Fock operator as the unperturbed Hamiltonian and the fluctuation potential as the perturbation. The wave function and the energy are expressed as a power series

$$\Psi = \sum_{i=0}^{n} \lambda^n \Psi^{(n)} \tag{2.25}$$

$$E = \sum_{i=0}^{n} \lambda^n E^{(n)} \tag{2.26}$$

The expansion is truncated, and the truncation level gives the order of perturbation. The zeroth, first, second and so forth order of perturbation theory are obtained when truncating at $\lambda^0, \lambda^1, \lambda^2$ and so forth. The first order energy correction term is given by

$$E^{(1)} = \langle \Psi^{(0)} | \hat{V} | \Psi^{(0)} \rangle \tag{2.27}$$

This is part of the Hartree-Fock energy because the Fock operator is the starting point. The second order energy correction is

$$E^{(2)} = \langle \Psi^{(0)} | \hat{V} | \Psi^{1)} \rangle \tag{2.28}$$

The Møller-Plesset perturbation theory is truncated at order n, thus yielding methods that are abbreviated as MPn. Second-order Møller-Plesset (MP2) is the most widely used. The working equation for MP2 energy calculations is written as

$$E_{MP2} = \frac{1}{4} \sum_{ij} \sum_{ab} t_{ij}^{ab} \langle ij||ab \rangle \tag{2.29}$$

where t_{ab}^{ij} is given by

$$t_{ij}^{ab} = \frac{\langle ij||ab \rangle}{\epsilon_i + \epsilon_j - \epsilon_a - \epsilon_b} \tag{2.30}$$

i and j denote occupied orbitals, a and b are virtual orbitals while ϵ_a, ϵ_b, ϵ_i and ϵ_j are the corresponding orbital energies. $\langle ij||ab \rangle = \langle ij|ab \rangle - \langle ij|ba \rangle$ are two-electron integrals.

2.3.4 Multi-Configurational Self-Consistent Field

In the multi-configurational approach, many electronic configurations or Slater determinants are used as the reference wave function. In this approach, one specify which set of molecular orbitals that are occupied in the reference configuration. One optimizes variationally both the coefficient of the determinants and the occupied molecular orbitals to obtain the electronic wave function giving the lowest energy.[45,46] The multi-configuration self-consistent field (MCSCF) approach requires that one consider the chemistry of the molecule when choosing the orbitals that are included in configurations of the reference wave function. This sometimes requires that one compute and analyse the orbitals of the molecule at a lower computational level of theory. The multiconfigurational second-order perturbation theory (CASPT2) is one of the mostly used multiconfiguration approaches for studies of the ground and excited states.[47]

2.4 Basis Sets

The basis set consists of a number of functions that are used for expanding the orbitals ($\psi_i(r)$) in electronic structure calculations.

$$\psi_i(r) = \sum_r c_j \phi_j(r) \tag{2.31}$$

In equation 2.31, $\phi_j(r)$ is a basis function and c_j is the molecular orbital coefficient. Originally Slater-type orbitals (STOs) were used to represent the atomic orbitals since they decay exponentially at long distances and near the nucleus similar to the wave function of the hydrogen atom.[48] However, the two-electron integrals of the STOs are difficult to compute. Boys realized that STOs could be approximated as linear combination of Gaussian-type orbitals (GTOs), rendering fast calculation of the two-electron integrals feasible.[49] GTOs can be written in terms of spherical coordinates as

$$G^{\zeta}_{nlm}(r,\theta,\phi) = Nr^{n-1}e^{-\zeta r^2}Y^m_l(\theta,\phi) \tag{2.32}$$

where N is a normalization constant, r is the distance from the nuclear position where the basis function is located, and $Y^m_l(\theta,\phi)$ is a spherical harmonic functions where n is the principal quantum number, l and m are angular momentum and magnetic quantum numbers, respectively.

The expansion in GTOs is not exact. However, it is possible to approach the basis set limit by systematically increasing the basis set size.[50,51] Most quantum chemical calculations use GTOs basis sets. Series of calculations employ for example double-ζ, triple-ζ, quadruple-ζ basis sets augmented with polarization and diffuse functions. For large molecules one has to use small to medium size basis set. In the calculations, we have mainly used the Karlsruhe triple-ζ quality basis sets (def2-TZVP) which is an accurate and compact basis set that can be used in studies of large molecules.[52,53]

2.5 Density Functional Theory

In density functional theory (DFT), one searches for an approximate solution to the Schrödinger equation by optimizing the electron probability density function (ρ) instead of the many-body wave function. The DFT method of today is based on the Kohn-Sham approach which is premised on the two Hohenberg-Kohn theorems, where they proved that the electron density is unique for any system of interacting particles in an external potential (V_{ext}). They also showed that the ground state energy (E_0) can be written as a functional of the ground state electron density (ρ).[54,55]

For non-interacting N-particle system, the many-body ground-state wave function is a single Slater determinant ($\Psi(r)$) constructed from a set of orbitals (ϕ)

$$\Psi(r) = \frac{1}{\sqrt{(N!)}} \begin{vmatrix} \phi_1(r_1) & \phi_2(r_1) & \cdots & \phi_N(r_1) \\ \phi_1(r_2) & \phi_2(r_2) & \cdots & \phi_N(r_2) \\ \vdots & \vdots & \cdots & \vdots \\ \phi_1(r_N) & \phi_2(r_N) & \cdots & \phi_N(r_N) \end{vmatrix} \tag{2.33}$$

The single-particle orbital $\phi_j(r)$ satisfy the Schrödinger equation

$$\Big(-\frac{\nabla^2}{2} + \mu_s(r) \Big) \phi_j(r) = \epsilon_j \phi_j(r) \tag{2.34}$$

The ground-state Kohn-Sham electron density is for the N-particle system is then expressed in terms of the orbitals as

$$\rho(r) = \sum_{j=1}^{N} |\phi(r)|^2 \tag{2.35}$$

The energy functional can then be expressed as

$$E[\rho(r)] = T_n[\rho(r)] + V_{ne}[\rho(r)] + V_{ee}[\rho(r)] + \Delta T[\rho(r)] + \Delta V_{ee}[\rho(r)] \tag{2.36}$$

T_n is the kinetic energy of non-interacting electrons
V_{ne} is the nuclear-electron interaction
V_{ee} is the electron-electron interaction
ΔT is a correction to the kinetic energy term due to the electron-electron interaction
ΔV_{ee} is the electron correlation contribution to the electron-electron repulsion

The kinetic energy of the non-interacting electrons (n) is given in terms of the Kohn-Sham orbitals ($\phi_i(r)$) by

$$T_n = -\frac{1}{2} \sum_{i}^{n} \int dr \phi_i^*(r) \nabla^2 \phi_i(r) \tag{2.37}$$

The nucleus-electron potential V_{ne}, and the classical electron-electron repulsion are de-

fined as in the Hartree-Fock theory. The remaining terms, ΔT and ΔV_{ee} are given by the exchange-correlation functional.

$$E_{XC}[\rho(r)] = \Delta T[\rho(r)] + \Delta V_{ee}[\rho(r)] \tag{2.38}$$

The construction of the exchange-correlation functional has used various approximations which has led to a rapidly expanding field of DFT research.[56–63] The functionals are grouped into local density, generalized-gradient approximation (GGA), meta-GGA, and hybrid functionals.

In the local density approximation (LDA), the E_{XC} is computed exclusively from the density (ρ) at some position r , and includes VWN correlation functional[64] in combination with Slater exchange functional.[54,55,65] The GGA functionals account for varying electron density by including the gradient of the electron density. The exchange-correlation energy is obtained from the sum of the exchange and correlation terms. The meta-GGA functionals include the second derivative of the electron density via the kinetic-energy density term. More advanced functionals are obtained by adding HF exchange to the functionals. Hybrid functionals have the same amount of HF for all electron-electron distances, whereas in range-separated functionals the amount of HF exchange differs at short and long inter-electronic distances.[66,67]

2.6 Time-Dependent Density Functional Theory (TDDFT)

The time-dependent density functional theory (TDDFT) is based on the Runge-Gross theorem[68] which states that for a given initial state, the time-dependent density is a unique functional of the external potential.

The derivation of TDDFT follows closely that of the time-dependent Hartree-Fock equation, except that in density functional theory, the time-dependent electron density, $\rho(r,t)$, is used instead of the time-dependent wave function. TDDFT can be formulated as a time-dependent Kohn-Sham DFT equation

$$i\frac{\partial\phi_i(r,t)}{\partial t} = \Big[-\frac{1}{2}\nabla^2 + \nu_s[\rho](r,t)\Big]\phi_i(r,t) \tag{2.39}$$

$\nu_s[\rho](r,t)$ is called the Kohn-Sham potential and is given by

$$\nu_s[\rho](r,t) = \nu_{ext}(r,t) + \nu_H[\rho](r,t) + \nu_{xc}[\rho](r,t) \tag{2.40}$$

Here, $\nu_{ext}(r,t)$ is the external field, $\nu_H[\rho](r,t)$ is the Hartree potential which accounts for the classical electrostatic interaction between the electrons, and $\nu_{xc}[\rho(r,t)]$ is the time-dependent exchange-correlation potential.

The time-dependent exchange-correlation potential ($\nu_{xc}[\rho(r,t)]$) is the difficult term to determine. In the adiabatic approximation, the potential is estimated using a functional of static DFT and evaluated as

$$\nu_{xc}[\rho(r,t)] \approx \frac{\partial E_{xc}}{\partial\rho}\Big|_{\rho=\rho(r,t)} \tag{2.41}$$

In many applications, linear response theory is sufficient to obtain the change in the electron density due to a time-dependent perturbation. Casida[69] derived a linear response equation for the calculation of excitation energies at the TDDFT level within the adiabatic approximation.

$$\begin{bmatrix} A & B \\ B^* & A^* \end{bmatrix} \begin{bmatrix} X \\ Y \end{bmatrix} = \omega \begin{bmatrix} 1 & 0 \\ 0 & -1 \end{bmatrix} \begin{bmatrix} X \\ Y \end{bmatrix} \tag{2.42}$$

Here ω is the excitation energy, X and Y are coefficients representing the response of the density with respect to the applied electric field and I is the unit matrix The expressions for the A and B matrices are

$$(A+B)_{ia\sigma,jb\sigma'} = (\epsilon_{a\sigma} - \epsilon_{i\sigma})\delta_{i,j}\delta_{a,b}\delta_{\sigma\sigma'} + 2(ia\sigma|jb\sigma') + 2f^{xc}_{ia\sigma,jb\sigma'} - c_x\delta_{\sigma\sigma'}[(ja\sigma|ib\sigma) + (ab\sigma|ij\sigma)] \tag{2.43}$$

and

$$(A-B)_{ia\sigma,jb\sigma'} = (\epsilon_{a\sigma} - \epsilon_{i\sigma})\delta_{i,j}\delta_{a,b}\delta_{\sigma\sigma'} + c_x\delta_{\sigma\sigma'}[(ja\sigma|ib\sigma) - (ab\sigma|ij\sigma)] \tag{2.44}$$

where $\epsilon_{i\sigma}$ and $\epsilon_{a\sigma}$ are the orbital energies of the occupied and virtual Kohn-Sham orbitals, $(pq\sigma|rs\sigma')$ is a two-electron integral in Mulliken notation and $f^{xc}_{ia\sigma,jb\sigma'}$ is a matrix element of the exchange-correlation kernel in the adiabatic approximation.

3 Magnetically Induced Current Densities

3.1 Quantum Theory of The Magnetic Fields

A classical particle with a charge of q and velocity of v will experience a Lorentz force, F in the presence of an electric field E and a magnetic field B.

$$F = q(E + v \times B) \tag{3.1}$$

The electric and magnetic field are described by Maxwell's equations which are given in differential form as

$$\nabla \cdot E = \frac{\rho}{\epsilon_o} \tag{3.2}$$

$$\nabla \cdot B = 0 \tag{3.3}$$

$$\nabla \times E = -\frac{\partial B}{\partial t} \tag{3.4}$$

$$\nabla \times B = \mu_o j \tag{3.5}$$

The four equations in 3.2, 3.3, 3.4 and 3.5 are also known as Gauss' law for electricity or the Coulomb's law, Gauss' law for magnetism, Faraday's law of induction, and Ampére's law, respectively. The symbols j, ρ, ϵ_o, μ_o stand for the current density, charge density, vacuum permittivity and permeability, respectively. The magnetic field can be expressed as the curl of a vector potential A of a homogeneous external magnetic field.

$$B = \nabla \times A \tag{3.6}$$

The vector potential A associated with an external magnetic field is defined as

$$A_0(r) = \frac{1}{2} B \times r_{i0} \tag{3.7}$$

where r_{i0} is the distance from the gauge origin r_0. The magnetic interaction of an intrinsic field due to a nuclear magnetic moment and an external magnetic field can be expressed using the generalized momentum operator $\hat{\pi} = p - A_0(r)$ inserted in the expression for the kinetic energy operator, $\hat{T}$, which then reads

$$T = \frac{1}{2}\pi^2 \tag{3.8}$$

where $\hat{p} = -i\nabla$ is the momentum operator. The current density $J(r)$ can be expressed in terms of the momentum operator as

$$J(r) = \frac{1}{2}(\Psi^* \hat{p} \Psi - \Psi \hat{p} \Psi^*) \tag{3.9}$$

where Ψ is the wave function. The current density in the presence of an external magnetic

field is given by

$$J(r) = \frac{1}{2}(\Psi^* \hat{p} \Psi - \Psi \hat{p} \Psi^* + A|\Psi|^2) \tag{3.10}$$

3.2 Aromaticity

When Michael Faraday isolated benzene in 1825,[70] the determination and understanding of its structure posed a great challenge to chemists. Though the empirical formula was long known, the determination of its cyclic structure is generally attributed to August Kekulé.[16] The term aromaticity was coined for benzene and other compounds because of their unusual stability and distinct odour.

Over the years the concept of aromaticity has evolved with several forms such as spherical aromaticity,[71,72] Möbius aromaticity,[73,74] Hückel aromaticity,[75] excited state aromaticity,[76] metalloaromaticity[77] etc. Currently there is no universal aromaticity definition,[78–80] although IUPAC's definition includes many aspects of aromaticity.[81] However, compounds that are considered aromatic have distinct electronic, structural, or chemical properties. The aforementioned form of aromaticity is based on the molecular electronic properties that are obtained by studying the electronic response in the presence of an external magnetic field.[82–84]

In the presence of an external magnetic field the electrons in a molecule will move around a molecule or part of the molecule leading to a magnetically induced current density in the molecule. According to Faraday's law, classically, the induced magnetic field will align in opposite direction to the external magnetic field. However, when quantum effects are considered, the induced magnetic field can also align with the direction of the external magnetic field. Aromaticity studies over the years have been based on investigation of the induced magnetic current generated by an external magnetic field.[85]

Quantum mechanical methods for studying magnetic interactions employ perturbation theory to calculate magnetically induced current density susceptibilities (MICDS). The external magnetic field is considered to be uniform and infinitely weak. Thus, the MICDS is calculated as the first order linear response to the applied external magnetic field, in the limit of zero field.

3.3 Gauge Including Magnetically Induced Current

The ring current concept was first introduced by London[86] in 1937, when he discussed interatomic currents and superconductivity of aromatic compounds. However, the seminal work of quantifying the intensity of the ring current was pioneered by Pople,[87] Coulson[88] and McWeeny.[89] By using the molecular orbital theory, Pople[87] and McWeeny[90] independently studied the ring current in aromatic compounds. Calculation and visual analyses of the current densities progressed with increasing computational power.[91] Current density profiles for benzene was reported by Atkins and Gomes.[92] However, calculations of current densities and visual presentation of these currents were hampered by the gauge-origin problem, which stems from the use of finite basis sets to represent molecular orbitals in the calculation of second-order molecular response magnetic properties.[93–95] The

gauge-origin problem was later tackled using the individual gauge for localized orbitals (IGLO)[95] and the gauge-including atomic orbital (GIAO)[96] approaches.

The individual gauge for localized orbital (IGLO) methods uses unique gauge origins for localized molecular orbitals associated with inner shell, bonding orbitals and lone pairs for the calculation of NMR chemical shifts. The gauge-including atomic orbitals (GIAO) on the other hand, uses atomic basis functions which are chosen such that they are dependent on the external magnetic field. The GIAO approach makes the calculation of nuclear shielding tensors independent of the origin. The gauge-including atomic orbitals are defined as

$$\chi_\mu(\mathbf{r}) = e^{-(\frac{i}{2})(\mathbf{B}\times[\mathbf{R}_\mu - \mathbf{R_o}])}\chi_\mu^{(0)}(\mathbf{r}) \tag{3.11}$$

where $\chi_\mu^{(0)}(\mathbf{r})$ is a standard Gaussian-type basis function. $\mathbf{R}_\mu$ and $\mathbf{R_o}$ denote the center of the basis function and the chosen gauge origin,respectively.

The gauge-including magnetically induced current (GIMIC) method[31,97] can be used for determining the degree of aromaticity using the ring-current criterion. GIMIC uses the strength of the ring current that is induced by the external magnetic field in a molecular ring to determine the degree of aromaticity. Aromatic rings sustain a net diatropic ring current whereas the net ring current of antiaromatic molecules are paratropic. The input required for GIMIC calculations are the one-electron unperturbed and perturbed density matrices, basis set information and the molecular structure data. The expression for calculating of the MICDS with the GIMIC approach is

$$\begin{aligned}\mathrm{J}_\upsilon^{\mathrm{B}_\tau\kappa}(\mathrm{r}) = &\sum_{\mu\nu} D_{\mu\nu}^\kappa \frac{\partial\chi_\mu^*(\mathrm{r})}{\partial \mathrm{B}_\tau}\frac{\partial\tilde{h}(\mathrm{r})}{\partial \mathrm{m}_\upsilon^k}\chi_\nu(\mathrm{r}) + \sum_{\mu\nu} D_{\mu\nu}^\kappa \chi_\mu^*\mathrm{r}\frac{\partial\tilde{h}(\mathrm{r})}{\partial \mathrm{m}_\upsilon^k}\frac{\partial\chi_\nu(\mathrm{r})}{\partial \mathrm{B}_\tau} \\ &+ \sum_{\mu\nu}\frac{\partial D_{\mu\nu}^\kappa}{\partial \mathrm{B}_\tau}\chi_\mu^*(\mathrm{r})\frac{\partial\tilde{h}(\mathrm{r})}{\partial \mathrm{m}_\upsilon^k}\chi_\nu(\mathrm{r}) - \sum_\delta \epsilon_{\upsilon\tau\delta}\left[\sum_{\mu\nu} D_{\mu\nu}^\kappa \chi_\mu^*\mathrm{r}\frac{\partial^2\tilde{h}(\mathrm{r})}{\partial \mathrm{m}_\upsilon^k \partial \mathrm{B}_\delta}\chi_\nu(\mathrm{r})\right]\end{aligned} \tag{3.12}$$

Here, B_τ is the external magnetic field and m_υ^k is the nuclear magnetic moment. $D_{\mu\nu}^\kappa$ and $\frac{\partial D_{\mu\nu}^\kappa}{\partial \mathrm{B}_\tau}$ are elements of the density matrix and the magnetically perturbed density matrices of α and β electrons (κ), respectively. $\frac{\partial^2\tilde{h}(\mathrm{r})}{\partial \mathrm{m}_\upsilon^k \partial \mathrm{B}_\tau}$ and $\frac{\partial\tilde{h}(\mathrm{r})}{\partial \mathrm{m}_\upsilon^k}$ describe the coupling between the external magnetic field and the nuclear magnetic moment. $\epsilon_{\upsilon\tau\delta}$ is the Levi-Civita permutation tensor and χ_ν denotes the basis function used.

When the MICDS is calculated on a grid, equation 3.12 can be reformulated in vector notation as

$$\mathrm{J}_\alpha^{B_\beta} = \mathbf{v^T P}_\beta \mathbf{d}_\alpha - \mathbf{b}_\beta^\mathbf{T}\mathbf{D}\mathbf{d}_\tau + \mathbf{v^T D q}_{\alpha\beta} - \epsilon_{\alpha\beta\gamma}\frac{\mathbf{1}}{\mathbf{2}}(\mathbf{v^T D v})\mathrm{r}_\gamma \tag{3.13}$$

where **D** is the atomic orbital (AO) density matrix, $\mathbf{P}_\alpha$ are the perturbed AO density matrices, **v** is the basis set vector, $\mathbf{r}_\gamma$ is a vector containing the grid points, and the basis set

derivatives $\mathbf{b}_\alpha$, $\mathbf{d}_\alpha$, $\mathbf{q}_{\alpha\beta}$ are given by

$$\mathbf{b}_\alpha = \frac{\partial \mathbf{v}}{\partial \mathbf{B}_\alpha} \tag{3.14}$$

$$\mathbf{d}_\alpha = \frac{\partial \mathbf{v}}{\partial \mathbf{r}_\alpha} \tag{3.15}$$

$$\mathbf{q}_{\alpha\beta} = \frac{\partial^2 \mathbf{v}}{\partial \mathbf{r}_\alpha \mathbf{B}_\beta} \tag{3.16}$$

with $(\alpha, \beta = x, y, z)$ The density matrices $\mathbf{D}$ and $\mathbf{P}_\alpha$ are obtained from standard *ab initio* and DFT calculations of nuclear magnetic shielding tensors. GIMIC is interfaced to Turbomole,[98,99] Cfour,[100] Gaussian[101] and QChem[102] for the studies of current densities using GIAOs.

3.4 Magnetically Induced Current Density Calculation

The GIMIC approach has the unique ability of quantifying the strength of both the paratropic and diatropic ring current sustained by a molecule. The ring-current strength susceptibility in the limit of zero magnetic field is obtained by integration of the current-density flow along selected bonds in a molecule. This feature of GIMIC has been used to quantify and classify whether molecules are aromatic, non-aromatic or anti-aromatic. The ring current of the archetypal benzene molecule has been reported to be 11.4 nA/T at the CCSD(T) level using a TZP basis set.[31] The approach has been used in studies of the aromaticity of polyaromatic hydrocarbons (PAHs),[103] porphyrinoids,[104] Möbius-twisted molecules,[105] and inorganic Al_4^{2-} and Al_4^{4-} compounds.[106]

In the present work, the GIMIC approach has been used to study the aromaticity of carbaporphyrinoids, porphycenes, and expanded porphyrins. The degrees of aromaticity of the compounds were obtained by calculating the ring-current strength and analyzing the current-density pathways. The studied molecules are multi-ring systems, whose aromatic character is not easily investigated by other means.

4 Photophysics

4.1 Electronic Excitations

When a molecule absorbs energy in the form of light, it can result in the promotion of an electron from a lower energy state to a higher one, or cause a chemical reaction by breaking chemical bonds. The later process is referred to as photochemistry, while the former one that is of interest in this thesis is referred to as photophysics.

The light-absorption process of molecules can be described using time-dependent perturbation theory. The electromagnetic radiation causes the initial wave function (Ψ) to evolve to a new wave function ($\Psi^{'}$). For such a transition, the transition dipole moment integral, μ is given by

$$\mu = \langle \Psi | \hat{\mu} | \Psi^{'} \rangle \tag{4.1}$$

The transition dipole moment, d, is separated into a sum of the electronic, μ_e and nuclei, μ_n components, $\mu = \mu_e + \mu_n$. The molecular wavefunction, Ψ, can be approximated as the product of the electronic (ψ_e) and nuclear (ψ_n) wavefunctions.

$$\Psi = \psi_e \psi_n \tag{4.2}$$

By substituting Equation 4.1 into 4.2,

$$\langle \Psi | \hat{\mu} | \Psi' \rangle = \int \int \psi_e{}^* \psi_n{}^* (\mu_e + \mu_n) \psi_e' \psi_n' d\tau_e d\tau_n \tag{4.3}$$

Equation 4.3 can be expanded to give

$$\langle \Psi | \hat{d} | \Psi' \rangle = \int \psi_n{}^* \psi_n' \left[\int \psi_e{}^* \mu_e \psi_e{}^* \right] d\tau_n + \int \psi_n{}^* \mu_n \psi_n' \left[\int \psi_e{}^* \psi_e' \right] \tau_e d\tau_n \tag{4.4}$$

The electronic wavefunction ψ_e depends parametrically on the nuclear coordinates, since $\psi_e{}^*$ and ψ_e' are orthogonal, the second term in equation 4.4 vanishes in Born-Oppenheimer approximation. Thus, the equation reduces to

$$\langle \Psi | \hat{\mu} | \Psi' \rangle = \int \psi_n{}^* \psi_n' \left[\int \psi_e{}^* \mu_e \psi_e' \right] d\tau_n \tag{4.5}$$

This indicates that an electronic transition will only be allowed if the term in the bracket is not equal to zero.

4.2 The Perrin-Jablonski Diagrams

The photophysical processes that occurs when a molecule absorbs a photon of UV-Vis radiation is summarized by a Jablonski[107] diagram shown in Figure 4.1.

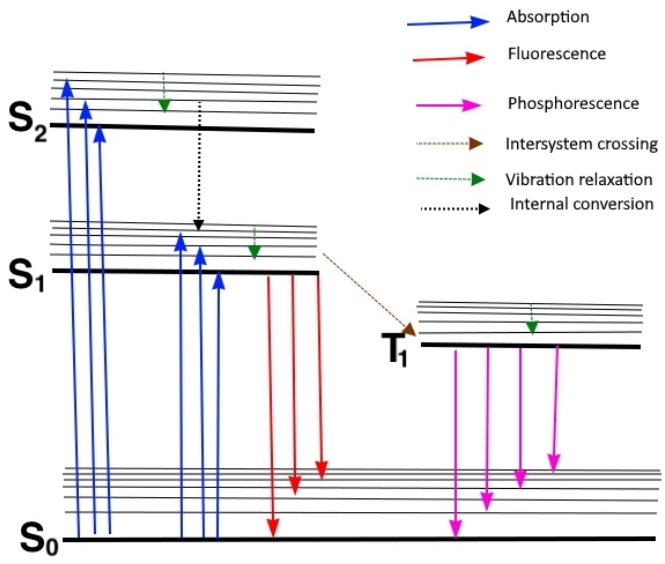

Figure 4.1: A Perrin-Jablonski diagram

4.2.1 Absorption

When a molecule absorbs a photon, an electron is excited from a lower energy state to a higher energy state. The energy of the absorbed photon must be equal to the energy difference between the states. The process is very fast and occurs on a femtosecond timescale. At ambient temperature, the excitation usually occurs from the lowest vibrational energy level. The intensity of the absorption bands is proportional to the square of the transition dipole moment.

4.2.2 Vibrational Relaxation

Molecular excited state strives towards energetically lower states. The excited molecule also loses some of its energy through structural relaxation and non-radiative processes. Vibrational relaxation, internal conversion (IC) and intersystem crossing (ISC) are non-radiative processes.

Vibrational relaxation implies a molecule in a higher vibrational energy level returns to a lower vibrational energy level by the dissipation of its energy to its environment. This can occur via intermolecular vibrational energy transfer or via a redistribution of the vibrational energy to other vibrational modes called intramolecular vibrational energy transfer. Vibrational relaxation is a very fast process occurring with a rate constant of 10^{11}s^{-1}–10^{12}s^{-1}

4.2.3 Internal Conversion and Intersystem Crossing

Internal conversion (IC) is the dissipation of energy between vibrational states of different electronic level. This happens as a result of overlap of the vibrational and electronic energy states in some molecules. The electronic states must have the same spin multiplicities. [108]

Intersystem crossing (ISC) is a radiationless process, which involves a transition between two electronic states with different spin multiplicities implying that there is a change of the spin state during the radiationless transition. Although ISC is a spin forbidden transition, it occurs nevertheless, due to a strong spin-orbit coupling that allows a spin-flip. Spin-orbit coupling is a relativistic effect that is large for molecules containing heavy elements. At the relativistic level of theory, spin is not a good quantum number, which implies that molecular states are not pure spin states rendering formally spin-forbidden transitions allowed.

4.2.4 Fluorescence

When an electron is excited to a higher electronic state with the same spin multipilicity, fluorescence is the radiative process by which the molecule loses energy. Fluorescence involves a de-excitation from a higher singlet state to the singlet ground state (S_0) accompanied by light emission. Usually, the de-excitation occurs from S_1 to S_0 following Kasha's rule, which states that photon emission occurs in appreciable yield mainly from the lowest excited state of a given multiplicity. [109]

Fluorescence quantum yield (ϕ_f) is the fluorescence efficiency relative to competing processes from the excited electronic states.

$$\phi_f = \frac{n_E}{n_A} \tag{4.6}$$

where n_A and n_E are the number of absorbed and emitted photons per unit time respectively. Generally, the fluorescence quantum yield is calculated in terms of the rate constant of radiative and non-radiative processes as

$$\phi_f = \frac{k_f}{k_f + \sum k_{nr}} \tag{4.7}$$

where k_f and $\sum k_{nr}$ are the rate constant for fluorescence and the sum of the rate constants of all competing non-radiative processes, respectively. [110]

4.2.5 Phosphorescence

The luminescent electronic transition from an excited triplet state to a singlet state is called phosphorescence. The triplet state is populated from the singlet manifold via intersystem crossing. The quantum yield of phosphorescence (ϕ_{ph}) is defined in terms of the rate of

radiative and non-radiative processes occurring from the triplet state.

$$\phi_{ph} = \frac{k_r^T}{k_r^T + k_{nr}^T}\phi_{isc} \tag{4.8}$$

where k_r^T and k_{nr}^T are the rate constant for radiative and non-radiative transition from the triplet state to the ground state, and ϕ_{isc} is the quantum yield of intersystem crossing which is defined as

$$\phi_{isc} = \frac{k_{isc}}{k_r + k_{nr}} \tag{4.9}$$

where k_r and k_{nr} are the rate constants of radiative and non-radiative transitions of the singlet states.

Phosphorescence is a slow process with a typical rate constant of $10^2 s^{-1}$ –$10^{-3} s^{-1}$. Phosphorescence emission generally occurs at a longer wavelength than fluorescence emission and absorption because the T_1 state is usually below the S_1 state.

4.3 Franck-Condon Principle

The Franck-Condon (FC) principle [111–113] gives a qualitative explanation for the intensities of the vibronic bands that are observed in highly resolved absorption spectra. The principle states that during an electronic transition, a change from one vibrational energy level of an electronic state to a vibrational state of another electronic state is more probable if the two vibrational wave functions have a large overlap. The FC principle is based on the fact that electronic transitions are much faster than the vibrational motion of the nuclei. The electronic transition can be considered to occur vertically between the two electronic states.

The quantum mechanical treatment of the FC principle starts with calculations of the expression for the transition dipole moment given in equation 4.1. [114] The interaction between the electronic and vibrational motion is neglected in equation 4.5 which gives the electronic contribution to the transition dipole moment multiplied with the overlap of the vibrational wave functions. Thus, in the FC approximation, the vibrational contribution to the transition dipole moment is

$$\mu_n = \int \psi_n{}^* \psi_n^{'} d\tau_n \tag{4.10}$$

yielding relative intensities of the bands observed in the absorption or emission spectra

4.4 Herzberg-Teller Approximation

The Herzberg-Teller approximation [115,116] goes beyond the FC approximation by accounting for changes in the electronic contribution to the transition moment with respect to changes in molecular structure.

The transition dipole moment is expanded in a Taylor series with respect to the normal coordinates of the vibrational modes.

$$\mu_{if}(Q) \simeq \mu_{if}(Q_0) + \sum_{k=1}^{N} \Big(\frac{\partial \mu_{if}}{\partial Q_k}\Big) Q_k + \frac{1}{2} \sum_{k=1}^{N} \sum_{l=1}^{N} \Big(\frac{\partial^2 \mu_{if}}{\partial Q_k Q_l}\Big) Q_k Q_l \tag{4.11}$$

where Q_0 is the equilibrium molecular structure, μ_{if} is the transition dipole moment. The partial derivatives consider changes in the transition dipole moment with respect to changes in the nuclear coordinate Q_k. The second term plays an important role for weakly allowed dipole-transitions with a small value for the first term in equation 4.11.

Truncating the expansion to include the first two terms gives the Herzberg-Teller approximation which explains observed bands in situations where $\mu_{if}(Q_0)$ is almost zero or vanishes for weakly allowed and dipole forbidden transitions, respectively.[38]

4.5 Duschinsky Mixing Effect

It may also be important to consider the nature of vibrational normal modes of the two electronic states.[117] For molecules whose initial and final electronic states significantly differ, the normal modes will also significantly differ which can be accounted for by introducing the mixing of the normal modes of the two states.

Duschinsky proposed that the normal modes of the involved states are related by a linear transformation. The normal mode of the final state (Q_f) can be expressed by rotating the normal coordinates of the initial state (Q_i) and shifting them with (K).[118]

$$Q_f = JQ_i + K \tag{4.12}$$

In equation 4.12, J is the Duschinsky rotation matrix and K is a geometric displacement vector.

4.6 Calculation of Vibrational Energies and Frequencies

It is possible to express the potential energy of a polyatomic molecule with 3N coordinate as a Taylor series about any local minima as

$$V(r_j) = V(0) + \sum_{j}^{N} \Big(\frac{\partial V}{\partial q_j}\Big) q_j + \frac{1}{2} \sum_{i,j} q_i \mathcal{H}_{i,j} q_j + \cdot \tag{4.13}$$

where $V(0)$ is the minimum energy of the molecule,
the second term $\sum_j^N \left(\frac{\partial V}{\partial q_j}\right) q_j$ is gradient of the energy along the q_j coordinate.

$\mathcal{H}_{i,j}$ is the second-derivative or Hessian matrix written as

$$\mathcal{H}_{i,j} = \frac{\partial^2 V}{\partial q_i \partial q_j} \tag{4.14}$$

The equation of motion for the atomic vibration can be expressed in a matrix form as

$$\frac{d^2q}{dt^2} = -Aq \tag{4.15}$$

where A is the mass-weighted Hessian matrix with matrix elements

$$A_{ij} = \frac{1}{m_j} H_{ij} \tag{4.16}$$

The normal modes and corresponding vibrational frequencies can be calculated once the mass-weighted Hessian matrix A is determined. The Hessian matrix will have 3N-5 and 3N-6 positive eigenvalues for linear and non-linear molecules, respectively. The eigenvalues of the Hessian matrix are squares of the so-called normal mode vibrational frequencies which are usually computed at the harmonic approximation.

4.7 Calculation of Absorption Spectra

In simulating the vibrationally resolved absorption spectra, two classes of methods at the Franck-Condon approximation are used.

Calculations in the frequency domain require explicit computation of Franck-Condon integrals between vibrational levels of the ground and the electronic excited state.[119,120] Even though the approach is straightforward, it is computationally expensive because of the large number of vibrational degrees of freedom. To reduce the number of Franck-Condon integrals that must be computed, pre-screening conditions have been introduced where only the relevant Franck-Condon integrals are explicitly computed.[121] The obtained spectrum is broadened using Gaussian or Lorentzian functions.

The time-domain approach circumvents explicit computations of Franck-Condon integrals by using a time-generating function introduced by Kubo.[122–126] A Fourier transform of the generating function yields the vibrational fine structure and Franck-Condon factors. The line broadening occurs as a result of the damping of the time-dependent function.

The absorption cross section for a transition from the lowest vibrational state of the initial electronic state i to a vibrational state in the final electronic state f in the Franck-Condon approximation is given by

$$\sigma_{abs}(\omega) = \frac{4\pi^2\omega}{3c}|\mu_{if}|^2 \sum_{vi}\sum_{vf} |\langle\psi_{vf}(\mathrm{Q}_f)|\psi_{vi}(\mathrm{Q}_i)\rangle|^2 \delta(E_{vf} - E_{vi} - \omega), \tag{4.17}$$

where ω is the transition energy, c is the speed of light, μ_{if} is the electronic transition dipole moment, v_i and v_f are vectors containing the vibrational quantum numbers for the initial and final vibrational states $\psi_{vi}(\mathrm{Q}_i)$ and $\psi_{vf}(\mathrm{Q}_f)$, respectively. $\delta(E_{vf} - E_{vi} - \omega$ ensures the energy conservation.

The vibrational wave functions of the ground and excited electronic states are approx-

imated as a product of one-dimensional harmonic oscillator wave functions given by

$$\psi_r(\mathrm{Q}_r) = \prod_j \chi_j(Q_j, v_j) = \prod_j |v_j\rangle \tag{4.18}$$

where r denotes the final or initial electronic state, and $\chi_j(Q_j)$ are one-dimensional harmonic oscillator wave functions, whose energies in the final and initial states are

$$E_{vi} = \frac{1}{2}\sum_j \omega_j^i \tag{4.19}$$

$$E_{vf} = \Delta E_{if} + \sum_j \left(\frac{1}{2} + v_j^f\right)\omega_j^f \tag{4.20}$$

where ω_j^i and ω_j^f are the vibrational energies in the ground and excited state, respectively, and ΔE_{if} is the adiabatic electronic excitation energy. Here, one assumes that only the lowest vibrational state of the initial electronic state is occupied.

The efficiency of the time-domain approach originates from the Fourier transform of the δ function. Equation 4.17 can then be written as

$$\sigma_{abs}(\omega) = \frac{4\pi^2\omega}{3c}|\mu_{if}|^2 \int_{\infty}^{-\infty} \mathrm{d}t\ \exp[-\mathrm{i}t(\Delta E_{vf} - E_{vi} - \omega)]G(t) \tag{4.21}$$

where $G(t)$ is the generating function for a molecule with N vibrational degrees of freedom. The generating function in Equation 4.21 is given by

$$G(t) = \sum_{vf} |\langle\psi_{vf}(Q_f)|\psi_{vi}(Q_i)\rangle|^2 \exp\left(-\mathrm{i}t\sum_j^N \left(v_j^f + \frac{1}{2}\right)\omega_j^f\right) \tag{4.22}$$

Calculation of the generating function in equation 4.22 includes all possible combinations of vibrational quantum numbers of the final states, defined by the quantum numbers in vector v_f and their vibrational frequencies ω_i^f. The approach is implemented in the RADLESS module of the TURBOMOLE program package.[4,98]

5 Results

5.1 Studied Molecules

5.1.1 Expanded Porphyrins

Expanded porphyrins are macrocycles consisting of more than four pyrrolic rings joined together directly or having one or two carbon atoms bridging the pyrrolic rings together.

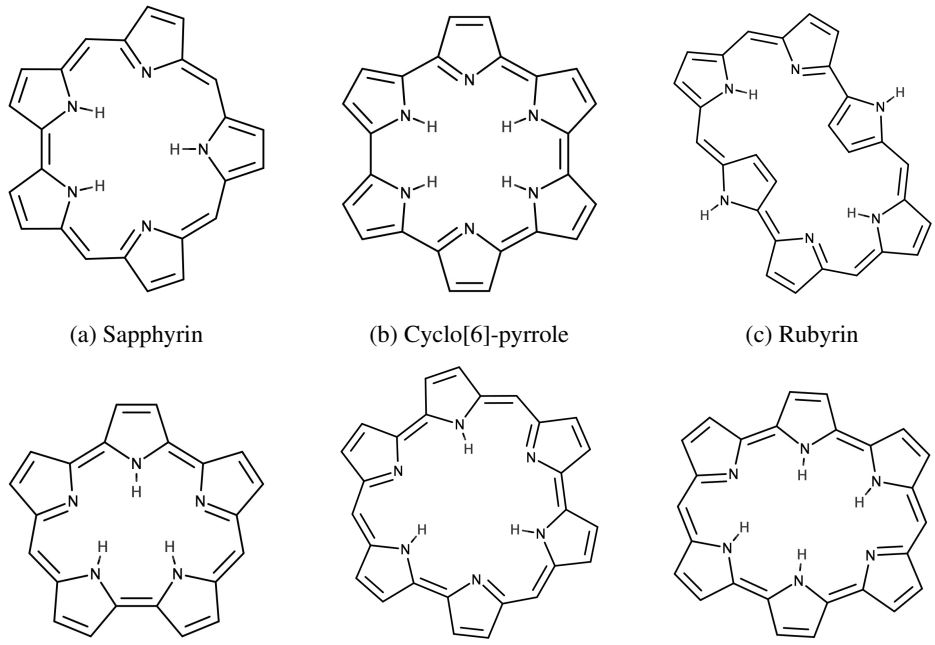

(a) Sapphyrin (b) Cyclo[6]-pyrrole (c) Rubyrin

(d) Orangarin (e) Rosarin (f) Amethyrin

Figure 5.1: The studied expanded porphyrins

The first expanded porphyrin reported in literature was sapphyrin shown in Figure 5.1a. Its name stems from its brightly blue colour. It was serendipitously obtained when Woodward *et al.* wanted to synthesize vitamin B_{12}.[127] Since then many synthetic routes have been reported.[128–130] The molecule in Figure 5.1b is cyclo[6]-pyrrole which has six pyrrolic rings that are directly linked at the α–carbon. Figure 5.1c shows rubyrin whose name originates from the Latin word *rubeus* because of the bright red colour of its diprotonated form. Sessler *et al.* reported the synthesis of an alkyl-substituted derivative of rubyrin.[131] Orangarin shown in Figure 5.1d is the smallest expanded porphyrin that has been reported.[132] It consists of five pyrrolic ring. Sessler *et al.* reported the synthesis of rosarin shown in Figure 5.1e.[133] Its name stems from the bright-red-to-purple colour of the triprotonated form. Amethyrin in Figure 5.1f has six pyrrolic rings with two methine (-CH) bridges and four directly fused pyrrolic rings.

5.1.2 Porphycenes

Porphycenes are porphyrin-like compounds with four linked pyrrolic rings. They were synthesized for the first time in the mid-1980s by Vogel *et al.*[134]

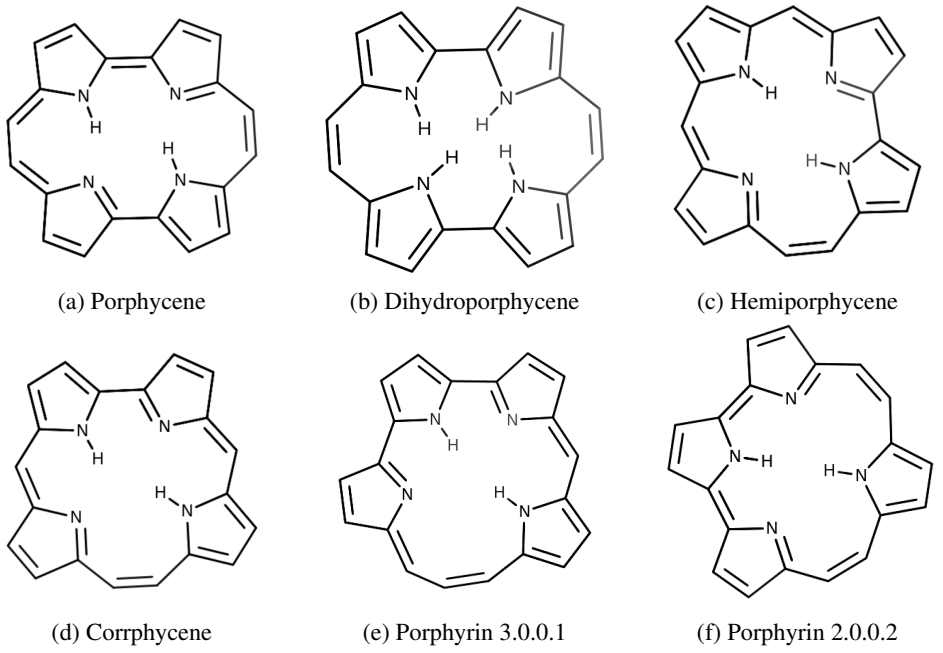

(a) Porphycene (b) Dihydroporphycene (c) Hemiporphycene

(d) Corrphycene (e) Porphyrin 3.0.0.1 (f) Porphyrin 2.0.0.2

Figure 5.2: The studied porphycenes

Porphycene in Figure 5.2a is a planar molecule with direct links between two of the pyrrole rings. The inner hydrogen can have two *cis* and one *trans* configuration. The lowest *cis* sturcture lies 2.7 kcal/mol above the *trans* conformer. Dihydroporphycene in Figure 5.2b has four inner hydrogens which distort the planarity of the molecule. It has a saddle-shaped structure where the inner hydrogens are bent outward. Ostapko *et al.* recently reported the synthesis of free-base hemiporphycene shown in Figure 5.2c.[135] The *trans* tautomer is the minimum energy structure. The molecular structure of corrphycene is shown in Figure 5.2d. It has one ethylidene bridge, two methine bridges and one direct link between pyrrolic rings. Sessler *et al.* first reported the synthesis of corrphycene.[136] The configuration with the inner hydrogens in *trans* position and the Z-configuration of the ethylidene bridge is energetically lowest structure. Porphyrin 3.0.0.1 and porphyrin 2.0.0.2 shown in Figure 5.2e and 5.2f, respectively are porphycenes that have been predicted by Waluk *et al.*[137] but to the best of my knowledge they have not yet been synthesized.

5.1.3 N-Doped Nanographenes

The molecular structure of the studied nanographenes are shown in Figure 5.3. A first look may suggest that they might have similar properties as polycyclic aromatic hydrocarbons. However, the presence of the nitrogen heteroatoms alters the chemistry of these compounds as shown in our work.[138]

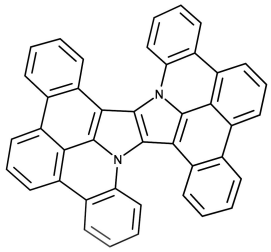

(a) Double [6]helicene

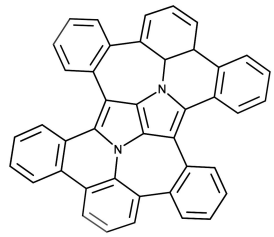

(b) Double [5]helicene

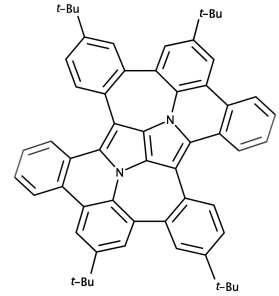

(c) Substituted double [5]helicene

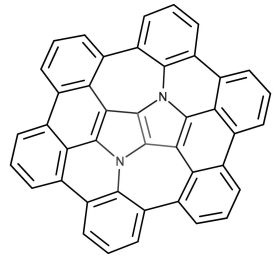

(d) diaza-nanographene

Figure 5.3: Molecular structure of the N-doped nanographenes

5.2 Aromatic Pathways

The gauge including magnetically induced current density (GIMIC) approach has been used to elucidate the aromatic pathways and the aromaticity of the studied molecules.

5.2.1 Expanded Porphyrins

By using the GIMIC approach, we confirmed that sapphyrin, cyclo-[6]-pyrrole and rubyrin are aromatic and they sustain ring-current strengths in the range of 24-30 nA/T, which is of same size as those of classical porphyrin.[104] The current-density pathway of the aromatic rubyrin is shown in Figure 5.4. Calculations of the ring-current strength using different DFT functionals yield similar values for the ring-current strengths. The ring current divides into an inner and outer pathways at the α–carbon atoms of the pyrrolic ring showing

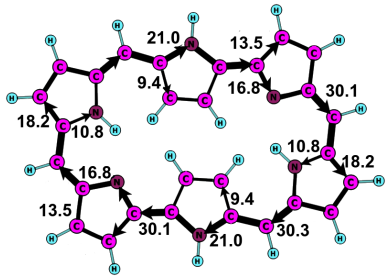

Figure 5.4: Current-density pathways and net ring current strength (in nA/T) passing selected bonds of rubyrin. The ring-current strengths were calculated at the B3LYP/def2-TZVP level of theory.

that all π-electrons of the pyrrolic rings participate in the aromatic pathway and contribute to the aromatic character.

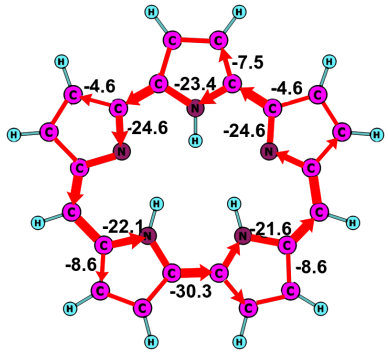

Figure 5.5: Current-density pathways and net ring-current strength (in nA/T) passing selected bonds of rosarin. The ring-current strengths were calculated at the MP2/def2-TZVP level of theory.

Orangarin, rosarin and amethyrin are antiaromatic according to the GIMIC calculations, which confirms the aromatic character that was deduced from experimental data.[139,140] However, the ring current strengths calculated using different DFT functionals differ substantially. Assuming that the *ab initio* MP2 method is the most reliable level of theory, hybrid functionals give the best result whereas pure DFT functionals tend to overestimate the strength of the paratropic ring current.

5.2.2 Porphycenes

Dihydroporphycene is an antiaromatic porphycene that is obtained by reducing the inner nitrogen atom of the pyrrolic rings with hydrogen atoms. The antiaromatic analogue of porphycene sustains a net paratropic ring current of -9 nA/T, whereas the pyrrolic rings sustain weak local diatropic ring current of 3 nA/T. Porphycene on the other hand sustains

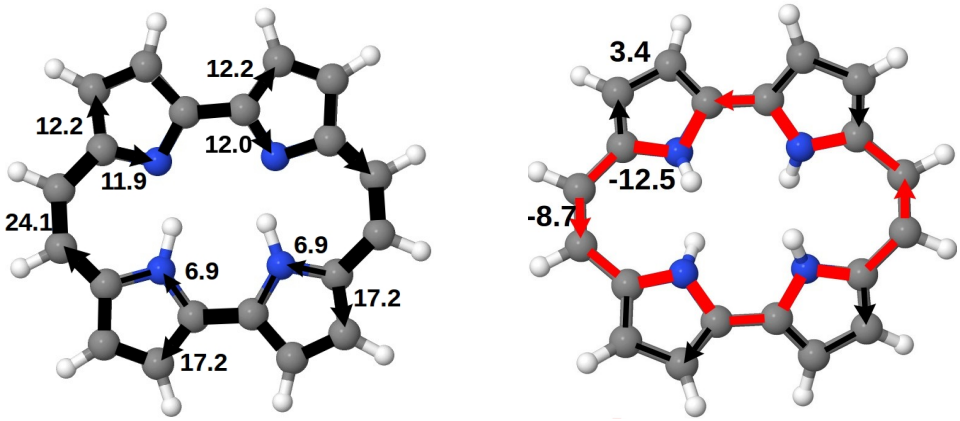

(a) (b)

Figure 5.6: Calculated ring-current strength and current pathways for (a) free-base *cis*-porphycene and (b) dihydroporphycene. The diatropic ring current is shown in black and the paratropic ring current is red. The ring-current strengths were calculated at the B3LYP/def2-TZVP level of theory

a net diatropic current of 24 nA/T, which is of the same size as for free-base porphyrin.[104] The current-density pathways of porphycene and dihydroporphycene are shown in Figure 5.6. Calculations of the vertical excitation energies showed that the antiaromatic dihydroporphycene has a smaller vertical excitation energy than the aromatic porphycene, even though the HOMO-LUMO gap of dihydroporphycene is larger for porphycene.

All other studied porphycene derivatives were aromatic according to GIMIC calculations. They sustain net diatropic ring-current strengths in the range of 17 – 26 nA/T. A comparison of the ^{1}H NMR shielding of the inner hydrogen atoms and the ring current strengths in these molecules did not show any clear correlation between the calculated ^{1}H NMR shielding and the ring current strength.

5.2.3 N-Doped Nanographenes

The current-density pathways in the N-doped nanographenes are a classical example of multi-ring systems, whose ring-current pathways and aromaticity are difficult to deduce from ^{1}H NMR studies. The calculated current-density pathways of the N-doped nanographenes offer insights into how the aromaticity of subrings of multiring systems can alternate between aromatic, non-aromatic and antiaromatic. The current-density also reveals how current-density pathways can split and join at molecular rings. The seven-membered antiaromatic ring weakens the global diatropic ring current. However, the peripheral six-membered benzene rings sustain a local diatropic ring current. Comparison of the ring-current strengths and pathways of the aza-nanographenes with polycyclic aromatic hydrocarbons (PAHs) like hexabenzocoronene (HBC), shows that the diatropic current that flows along the edge of the aza-nanographene is much weaker than for HBC.

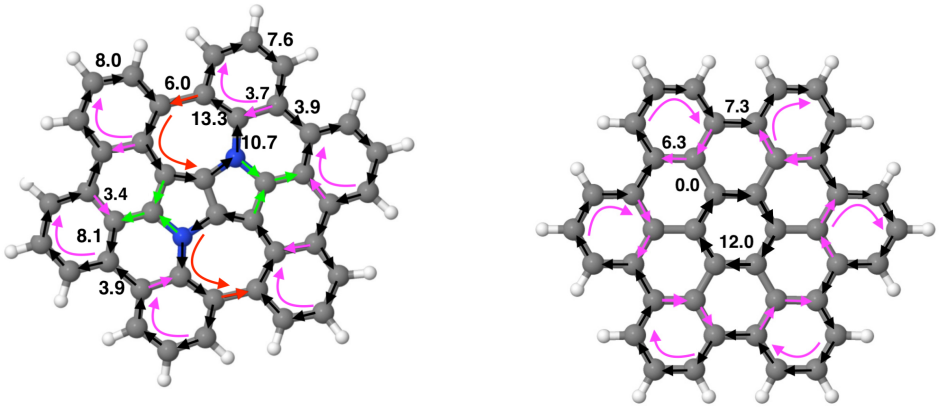

(a) (b)

Figure 5.7: Calculated ring-current strength and current-density pathways for (a) double [6]helicene and (b) hexabenzocoronene. The ring-current strengths were calculated at the B3LYP/def2-TZVP level of theory. The bent arrows illustrate local ring currents, whereas the arrows along the bonds show the flux of the current density.

The outer benzene rings sustain weak diatropic ring current in both molecules.

5.3 Rate Constants and Quantum Yield

Calculations of rate constants for non-radiative transitions require computing accurate energy differences between the involved electronic states. Vertical excitation energies calculated at *ab initio* and TDDFT levels of theory showed that the energy of the S_1 state of the aromatic expanded porphyrins are overestimated at the CC2 and TDDFT levels of theory, whereas XMC-QDPT2 calculations, on the other hand, underestimate the vertical excitation energy of the S_1 state. For the antiaromatic molecules the excitation energy of S_1 state calculated at the CC2, TDDFT and XMC-QDPT2 levels agrees well with experimental data.[139,141]

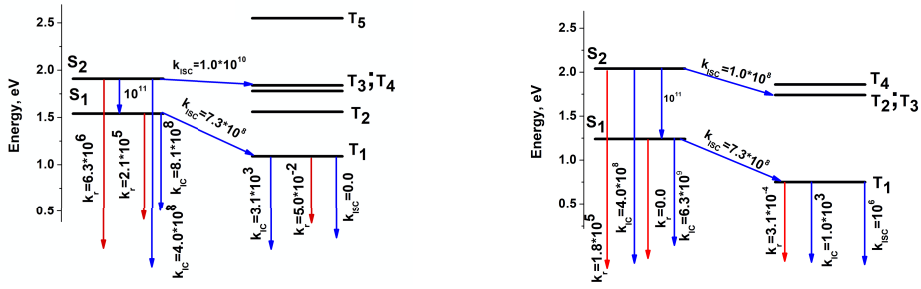

Figure 5.8: Calculated rate constants for (a) aromatic sapphyrin and (b) antiaromatic rosarin

The energy dissipation pathways were studied for the expanded porphyrins by calculating the rate constants for internal conversion (IC), intersystem crossing (ISC), fluorescence and phosphorescence. The rate constant calculations for aromatic sapphyrin, show that the IC rate from S_1 to S_0 is as fast as the ISC process from S_1 to T_1. The ISC process from S_2 to T_4 is a factor of 10 slower and the IC from S_2 to S_0 is about 250 times slower. The fluorescence rate is much slower in this molecule. The rate constant calculations of rosarin show that the decay from the S_2 state is dominated by internal conversion. There is a fast internal conversion (IC) process from the S_1 to the S_0 state for the antiaromatic molecules. Though fluorescence from the S_1 has been experimentally detected,[141] our calculation shows that the rate is slower. Omitting the Herzberg-Teller effect in the calculation may lead to underestimation of the radiative transitions probabilities.

5.4 Vibrationally Resolved Absorption Spectra

The absorption spectra of naphthalene, anthracene, pentacene and pyrene were simulated at the zeroth-order Franck-Condon approximation using the approach based on the time-generating function, which is an efficient approach that does not require any calculation of individual Franck-Condon factors. Excitation energies calculated at the CC2 and ADC2 levels for the molecules were in good agreement with those of experimental values. The excitation energies calculated at the TDDFT level using the Becke-half-and-half (BH-LYP) functional are larger than the ones obtained using the Perdew-Burke-Ernzerhof hybrid (PBE0) functional, suggesting that a larger amount of Hartree-Fock exchange in the functional leads to a blue shift of calculated vertical excitation energies that are also larger than the experimental values.[142–145]

The vibrationally resolved absorption spectrum of pentacene in Figure 5.9 obtained with the RADLESS code is qualitatively similar to the experimental one. The 0–0 transition energy is 0.57 eV smaller than the experimental one. A more accurate 0–0 transition energy is expected at the CC2 level, because the vertical excitation energy is 0.38 eV larger than the vertical excitation energy calculated using the PBE0 functional. However, by introducing a shift of 0.57 eV, we obtained at the PBE0 level a nearly perfect agreement between the simulated and experimental absorption spectra of pentacene.

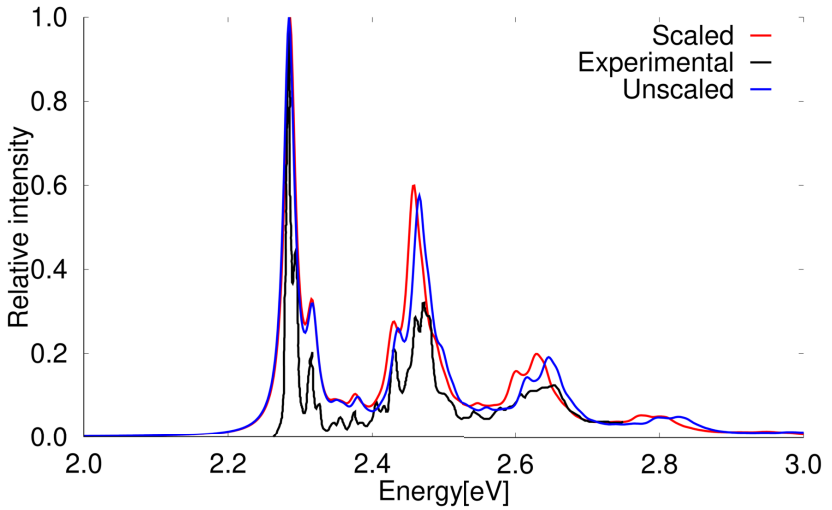

Figure 5.9: Vibrationally resolved absorption spectrum of the $1B_{2u}$ state of pentacene calculated at the PBE0 level. The experimental spectrum is taken from ref. 146

Comparing higher vibrational bands of the simulated spectra to those of experimental ones shows that there is a blue shift of the simulated spectra, because vibrational frequencies are often overestimated in the harmonic approximation. A better agreement is obtained using a scaling factor to slightly reduce the vibrational energies obtained in the harmonic approximation. In the scaled spectrum in Figure 5.9, the vibrationally energies

have been multiplied by a factor of 0.95. The scaled spectrum agrees very well with the experimental one.

The vibrational bands of the absorption spectrum can be assigned to mode or combination modes of the vibrational frequencies. This is done by identifying the totally symmetric irreducible representation of the point group. The energy difference between a given vibrational band and the 0–0 transition energy corresponds to the energy of the vibrational frequency of the totally symmetric irreducible representation or to the sum of the energy of the vibrational frequencies. The assignment of the individual vibrational peaks of the $1B_{2u}$ state of pentacene is shown in Table 5.1

Table 5.1: Assignment of the vibrational peaks in the absorption spectrum of pentacene calculated at the PBE0 level. The vibrational bands originate from transitions involving the totally symmetric (A_g) vibrational modes of the $1B_{2u}$ excited state. The transition energies (in eV), the vibrational shift of the transition energies (in cm^{-1}) and the relative intensities are reported.

Energy (in eV)	Shift (in cm^{-1})	Relative intensity	Assignment
2.286	0	1.000	0–0
2.319	265	0.245	15 A_g
2.381	767	0.052	39 A_g
2.433	1184	0.082	64 A_g
2.438	1226	0.117	68 A_g
2.462	1417	0.141	78 A_g
2.467	1460	0.331	81 A_g
2.479	1522	0.144	85 A_g
2.484	1560	0.028	87 A_g
2.494	1653	0.036	
2.500	1680	0.076	15 A_g + 78 A_g
2.512	1787	0.034	15 A_g + 85 A_g
2.614	2621	0.041	60 A_g + 87 A_g
2.619	2662	0.039	60 A_g + 90 A_g
2.643	2855	0.044	75 A_g + 85 A_g
2.648	2896	0.056	75 A_g + 87 A_g
2.660	2992	0.049	

6 Summary and Conclusions

The concept of aromaticity continues to evolve because novel aromatic and antiaromatic molecules are synthesized. Expanded porphyrins belong to a class of molecules that has received much attention because of their potential use in technological devices[147–149] In Article I, the aromatic and photophysical properties of selected expanded porphyrins were studied. The ring-current pathways were elucidated using the GIMIC approach. The study showed that the lowest electronic transition in antiaromatic expanded porphyrins is a magnetic transition leading to the strong paratropic ring-current of the antiaromatic expanded porphyrins. The calculated rate constants show that the energy dissipation pathways is dominated by IC for the studied molecules.

Porphycene and porphycene derivatives are porphyrin analogues of interest because of their unique structure making them good candidates for use as sensitizers for photodynamic therapy, in catalysis, and as dyes in solar cells.[150–153] Article II provides insights into the ring-current strength and pathways. The poprhycene studies in Article II showed that the interaction between the inner hydrogens and inner nitrogen were more significant for difference in the observed ^{1}H NMR chemical shift than the global ring current.

The vibrational modes that contribute to the absorption spectrum of anthracene, naphthalene, pentacene and pyrene have been calculated using the RADLESS approach where a time-generating function is used at the Franck-Condon level. The calculations show that the method is very efficient for simulating vibrationally resolved absorption spectra that are very reminiscent of the experimental. This study is presented in Article III.

The aromatic character of N-doped nanographenes has been studied in Article IV. The current-density pathways of N-doped nanographenes differ from that of PAHs. The N-doped nanographenes have weak diatropic current at the edges of the molecules, whereas the edge current is very strong in PAHs. The local and global ring-current strengths have been calculated. In the N-doped nanographenes with a seven-membered subring, local ring-current strength alternate between aromatic, nonaromatic and antiaromatic in the subring.

7 References

[1] Dierksen, M.; Grimme, S. *J. Chem. Phys.* **2004**, *120*, 3544–3554.

[2] Santoro, F.; Improta, R.; Lami, A.; Bloino, J.; Barone, V. *J. Chem. Theory Comput.* **2007**, *126*, 084509.

[3] Karasulu, B.; Götze, J. P.; Thiel, W. *J. Chem. Theory Comput.* **2014**, *10*, 5549–5566.

[4] Tapavicza, E.; Furche, F.; Sundholm, D. *J. Chem. Theory Comput.* **2016**, *12*, 5058–5066.

[5] Zuehlsdorff, T. J.; Isborn, C. M. *Int. J. Quantum Chem.* **2019**, *119*, e25719.

[6] Begušić, T.; Vaníček, J. *J. Chem. Phys.* **2020**, *153*, 024105.

[7] Tavernelli, I.; Röhrig, U. F.; Rothlisberger, U. *Mol. Phys.* **2005**, *103*, 963–981.

[8] Tapavicza, E.; Bellchambers, G. D.; Vincent, J. C.; Furche, F. *Phys. Chem. Chem. Phys.* **2013**, *15*, 18336–18348.

[9] Brunk, E.; Röthlisberger, U. *Chem. Rev.* **2015**, *115*, 6217–6263.

[10] Suomivuori, C.-M.; Gamiz-Hernandez, A. P.; Sundholm, D.; Kaila, V. R. I. *Proc. Natl. Acad. Sci. (USA)* **2017**, *114*, 7043–7048.

[11] Davidson, E. R.; Jarzecki, A. A. *Chem. Phys. Letters* **1998**, *285*, 155–159.

[12] Nitzsche, L. E.; Davidson, E. R. *J. Am. Chem. Soc.* **1978**, *100*, 7201–7204.

[13] Loos, P.-F.; Scemama, A.; Jacquemin, D. *J. Phys. Chem. Lett.* **2020**, *11*, 2374–2383.

[14] Brückner, C.; Engels, B. *J. Phys. Chem. A* **2015**, *119*, 12876–12891.

[15] TURBOMOLE V7.2 2017, a development of University of Karlsruhe and Forschungszentrum Karlsruhe GmbH, 1989-2007, TURBOMOLE GmbH, since 2007; available from `http://www.turbomole.com`.

[16] Kekulé, A. *Bull. Soc. Chim.* **1865**, *3*, 98–110.

[17] Berger, R. J. F.; Viel, A. *Z. Naturforsch. B* **2020**, *75*, 327–339.

[18] Liu, C.; Ni, Y.; Lu, X.; Li, G.; Wu, J. *Acc. Chem. Res.* **2019**, *52*, 2309–2321.

[19] Kopp, S. M.; Gotfredsen, H.; Deng, J.-R.; Claridge, T. D.; Anderson, H. L. *J. Am. Chem. Soc.* **2020**, *142*, 19393–19401.

[20] Baryshnikov, G. V.; Valiev, R. R.; Kuklin, A. V.; Sundholm, D.; Ågren, H. *J. Phys. Chem. Lett.* **2019**, *10*, 6701–6705.

[21] Valiev, R. R.; Fliegl, H.; Sundholm, D. *Phys. Chem. Chem. Phys.* **2015**, *17*, 14215–14222.

[22] Lash, T. D. *Angew. Chem. Int. Ed.* **1995**, *34*, 2533–2535.

[23] Benkyi, I.; Fliegl, H.; Valiev, R. R.; Sundholm, D. *Phys. Chem. Chem. Phys.* **2016**, *18*, 11932–11941.

[24] Krygowski, T. M.; Cyrański, M. K. *Chem. Rev.* **2001**, *101*, 1385–1420.

[25] Randic, M. *J. Am. Chem. Soc.* **1977**, *99*, 444–450.

[26] Kumar, C.; Fliegl, H.; Sundholm, D. *J. Phys. Chem. A* **2017**, *121*, 7282–7289.

[27] Mo, Y.; Schleyer, P. v. R. *Chem. Eur. J.* **2006**, *12*, 2009–2020.

[28] Cyranski, M. K.; Krygowski, T. M.; Katritzky, A. R.; Schleyer, P. v. R. *J. Org. Chem.* **2002**, *67*, 1333–1338.

[29] Stanger, A. *Chem. Comm.* **2009**, 1939–1947.

[30] Fliegl, H.; Valiev, R.; Pichierri, F.; Sundholm, D. *Chemical Modelling: Volume 14*; The Royal Society of Chemistry, 2018; Vol. 14; pp 1–42.

[31] Jusélius, J.; Sundholm, D.; Gauss, J. *J. Chem. Phys.* **2004**, *121*, 3952–3963.

[32] Valiev, R. R.; Fliegl, H.; Sundholm, D. *J. Phys. Chem. A* **2013**, *117*, 9062–9068.

[33] Taubert, S.; Jusélius, J.; Sundholm, D.; Klopper, W.; Fliegl, H. *J. Phys. Chem. A* **2008**, *112*, 13584–13592.

[34] Valiev, R. R.; Fliegl, H.; Sundholm, D. *J. Phys. Chem. A* **2015**, *119*, 1201–1207.

[35] Schrödinger, E. *Ann. Phys.* **1926**, *385*, 437–490.

[36] Born, M.; Oppenheimer, R. *Ann. Phys.* **1927**, *389*, 457.

[37] Fischer, G. *Vibronic coupling: The interaction between the electronic and nuclear motions*; Academic Press, 1984; Vol. 9.

[38] Baer, M. *Beyond Born-Oppenheimer: electronic nonadiabatic coupling terms and conical intersections*; John Wiley & Sons, 2006.

[39] Fock, V. *Z. Physik* **1930**, *61*, 126.

[40] Hartree, D. R. *Proc. Cambridge Phil. Soc.* **1928**, *24*, 89.

[41] Roothaan, C. C. J. *Rev. Mod. Phys.* **1951**, *23*, 69.

[42] Szabo, A.; Ostlund, N. S. *Modern Quantum Chemistry: Introduction to Advanced Electronic Structure Theory*; Dover Publications Inc., 2012.

[43] Christiansen, O.; Koch, H.; Jørgensen, P. *Chem. Phys. Letters* **1995**, *243*, 409–418.

[44] Møller, C.; Plesset, M. S. *Phys. Rev.* **1934**, *46*, 618–622.

[45] Hinze, J. *J. Chem. Phys.* **1973**, *59*, 6424–6432.

[46] Hinze, J.; Roothaan, C. C. J. *Prog. Theor. Phys.* **1967**, *40*, 37–51.

[47] Finley, J.; Malmqvist, P.-Å.; Roos, B. O.; Serrano-Andrés, L. *Chem. Phys. Letters* **1998**, *288*, 299–306.

[48] Slater, J. C. *Phys. Rev.* **1930**, *36*, 57–64.

[49] Boys, S. F. *Proc. Roy. Soc.* **1950**, *200*, 542.

[50] Martin, J. M. L. *Chem. Phys. Letters* **1996**, *259*, 669–678.

[51] Helgaker, T.; Klopper, W.; Koch, H.; Noga, J. *J. Chem. Phys.* **1997**, *106*, 9639–9646.

[52] Schäfer, A.; Huber, C.; Ahlrichs, R. *J. Chem. Phys.* **1994**, *100*, 5829–5835.

[53] Weigend, F.; Ahlrichs, R. *Phys. Chem. Chem. Phys.* **2005**, *7*, 3297–3305.

[54] Hohenberg, P.; Kohn, W. *Phys. Rev.* **1964**, *136*, B864–B871.

[55] Kohn, W.; Sham, L. J. *Phys. Rev.* **1965**, *140*, A1133–A1138.

[56] Tao, J.; Perdew, J. P.; Staroverov, V. N.; Scuseria, G. E. *Phys. Rev. Letters* **2003**, *91*, 146401.

[57] Perdew, J. P.; Chevary, J. A.; Vosko, S. H.; Jackson, K. A.; Pederson, M. R.; Singh, D. J.; Fiolhais, C. *Phys. Rev. B* **1993**, *48*, 4978–4978.

[58] Perdew, J. P.; Burke, K.; Wang, Y. *Phys. Rev. B* **1996**, *54*, 16533–16539.

[59] Becke, A. D. *Phys. Rev. A* **1988**, *38*, 3098–3100.

[60] Lee, C.; Yang, W.; Parr, R. G. *Phys. Rev. B* **1988**, *37*, 785–789.

[61] Miehlich, B.; Savin, A.; Stoll, H.; Preuss, H. *Chem. Phys. Letters* **1989**, *157*, 200–206.

[62] Perdew, J. P.; Burke, K.; Ernzerhof, M. *J. Chem. Phys.* **1996**, *105*, 9982–9985.

[63] Zhao, Y.; Truhlar, D. G. *J. Chem. Phys.* **2006**, *125*, 194101.

[64] Vosko, S. H.; Wilk, L.; Nusair, M. *Can. J. Phys* **1980**, *58*, 1200–1211.

[65] Slater, J. C.; Phillips, J. C. *Phys. Today* **1974**, *27*, 49–50.

[66] Vydrov, O. A.; Scuseria, G. E. *J. Chem. Phys.* **2006**, *125*, 234109.

[67] Gerber, I. C.; Angyán, J. G. *Chem. Phys. Letters* **2005**, *415*, 100–105.

[68] Runge, E.; Gross, E. K. U. *Phys. Rev. Letters* **1984**, *52*, 997–1000.

[69] Casida, M. E. *Recent Advances In Density Functional Methods: (Part I)*; World Scientific, 1995; pp 155–192.

[70] Faraday, M. *Phil. Trans. Roy.* **1825**, 440.

[71] Hirsch, A.; Chen, Z.; Jiao, H. *Angew. Chem. Int. Ed.* **2000**, *39*, 3915–3917.

[72] Bühl, M.; Hirsch, A. *Chem. Rev.* **2001**, *101*, 1153–1183.

[73] Rzepa, H. S. *Chem. Rev.* **2005**, *105*, 3697–3715.

[74] Heilbronner, E. *Tetrahedron Lett.* **1964**, *5*, 1923–1928.

[75] Hückel, E. *Z. Physik* **1931**, *70*, 204–286.

[76] Baird, N. C. *J. Am. Chem. Soc.* **1972**, *94*, 4941–4948.

[77] Masui, H. *Coord. Chem. Rev.* **2001**, *219-221*, 957–992.

[78] von Ragué Schleyer, P.; Jiao, H. *Pure Appl. Chem.* **1996**, *28*, 209.

[79] Hoffmann, R. *Am. Sci* **2015**, *103*, 1511.

[80] Solà, M. *Front. Chem.* **2017**, *5*, 22.

[81] IUPAC. Compendium of Chemical Terminology, 2nd ed. (the "Gold Book"). Compiled by A. D. McNaught and A. Wilkinson. Blackwell Scientific Publications, Oxford (1997). Online version (2019-) created by S. J. Chalk. ISBN 0-9678550-9-8. https://doi.org/10.1351/goldbook.

[82] von Ragué Schleyer, P.; Maerker, C.; Dransfeld, A.; Jiao, H.; van Eikema Hommes, N. J. R. *J. Am. Chem. Soc.* **1996**, *118*, 6317–6318.

[83] Chen, Z.; Heine, T.; Sundholm, D.; von Ragué Schleyer, P. In *Quantum Chemical Calculation of Magnetic Resonance Properties*; Kaupp, M., Bühl, M., Malkin, V., Eds.; Wiley-VCH: Weinheim, Germany, 2004; pp 395–407.

[84] Wannere, C. S.; Corminboeuf, C.; Allen, W. D.; Schaefer III, H. F.; von Ragué Schleyer, P. *Org. Letters* **2005**, *7*, 1457–1460.

[85] Sundholm, D.; Fliegl, H.; Berger, R. J. F. *WIREs Comput. Mol. Sci.* **2016**, *6*, 639–678.

[86] London, F. *J. Phys. Radium* **1937**, *8*, 397–409.

[87] Pople, J. A. *J. Chem. Phys.* **1956**, *24*, 1111.

[88] C. A. Coulson, J. A. N. F. Gomes and R. B. Mallion, *Mol. Phys* **1975**, *30*, 713.

[89] McWeeny, R. *Mol. Phys.* **1958**, *1*, 311–321.

[90] Pople, J. A. *Mol. Phys.* **1958**, *1*, 175–180.

[91] Hegstrom, R.; Lipscomb, W. *J. Chem. Phys.* **1968**, *48*, 809–811.

[92] Atkins, P.; Gomes, J. *Mol. Phys.* **1976**, *32*, 1063–1074.

[93] Helgaker, T.; Jaszuński, M.; Ruud, K. *Chem. Rev.* **1999**, *99*, 293–352.

[94] Malkin, M. K. M. B. V. G. *Calculation of NMR and EPR parameters : theory and applications*; Wiley-VCH, 2004.

[95] Kutzelnigg, W.; van Wüllen, C.; Fleischer, U.; Franke, R.; van Mourik, T. In *Nuclear Magnetic Shieldings and Molecular Structure*; Tossell, J. A., Ed.; Kluwer Academic Publishers, 1993; pp 141–161.

[96] Cheeseman, J. R.; Trucks, G. W.; Keith, T. A.; Frisch, M. J. *J. Chem. Phys.* **1996**, *104*, 5497–5509.

[97] Fliegl, H.; Taubert, S.; Lehtonen, O.; Sundholm, D. *Phys. Chem. Chem. Phys.* **2011**, *77*, 3408–3414.

[98] Ahlrichs, R.; Bär, M.; Häser, M.; Horn, H.; Kölmel, C. *Chem. Phys. Letters* **1989**, *162*, 165–169, current version: see http://www.turbomole.com.

[99] Furche, F.; Ahlrichs, R.; Hättig, C.; Klopper, W.; Sierka, M.; Weigend, F. *WIREs Comput. Mol. Sci.* **2014**, *4*, 91–100.

[100] Stanton, J. F.; Gauss, J.; Harding, M. E.; Szalay, P. G. 2009; CFOUR, Coupled Cluster techniques for Computational Chemistry, a quantum-chemical program package also with contributions from A.A. Auer, R.J. Bartlett, U. Benedikt, C. Berger, D.E. Bernholdt, Y.J. Bomble, O. Christiansen, M. Heckert, O. Heun, C. Huber, T.-C. Jagau, D. Jonsson, J. Jusélius, K. Klein, W.J. Lauderdale, D.A. Matthews, T. Metzroth, D.P. O'Neill, D.R. Price, E. Prochnow, K. Ruud, F. Schiffmann, S. Stopkowicz, M.E. Varner, J. Vázquez, F. Wang, J.D. Watts and the integral packages MOLECULE (J. Almlöf and P.R. Taylor), PROPS (P.R. Taylor), ABACUS (T. Helgaker, H.J. Aa. Jensen, P. Jørgensen, and J. Olsen), and ECP routines by A. V. Mitin and C. van Wüllen. For the current version, see http://www.cfour.de.

[101] Frisch, M. J. et al. Gaussian 03 (Revision B.03). 2003.

[102] Shao, Y. et al. *Phys. Chem. Chem. Phys.* **2006**, *8*, 3172–3191.

[103] Kaipio, M.; Patzschke, M.; Fliegl, H.; Pichierri, F.; Sundholm, D. *J. Phys. Chem. A* **2012**, *116*, 10257–10268.

[104] Fliegl H. and Sundholm D., *J. Org. Chem.* **2012**, *77*, 3408–3414.

[105] Fliegl, H.; Sundholm, D.; Pichierri, F. *Phys. Chem. Chem. Phys.* **2011**, *13*, 20659–20665.

[106] Fliegl, H.; Lehtonen, O.; Patzschke, M.; Sundholm, D.; Lin, Y. C. *Theoret. Chem. Acc.* **2011**, *129*, 701–713.

[107] A, J. *Nature* **1933**, *131*, 839–840.

[108] Rohatgi-Mukherjee, K. K. *Fundamentals of Photochemistry*; New Age International, 1978.

[109] Kasha, M. *Discuss. Faraday Soc.* **1950**, *9*, 14–19.

[110] Balzani, V.; Ceroni, P.; Juris, A. *Photochemistry and Photophysics: Concepts, Research, Applications*; John Wiley & Sons, 2014.

[111] Franck, J.; Dymond, E. G. *Trans. Faraday Soc.* **1926**, *21*, 536–542.

[112] Condon, E. U. *Phys. Rev.* **1928**, *32*, 858.

[113] Condon, E. *Phys. Rev.* **1926**, *28*, 1182.

[114] Lax, M. *J. Chem. Phys.* **1952**, *20*, 1752–1760.

[115] Herzberg, G.; Teller, E. *Z. Physik. Chem.* **1933**, *21B*, 410–446.

[116] Herzberg, G. *Electronic spectra and electronic structure of polyatomic molecules*; Van Nostrand: New York, 1966.

[117] Small, G. J. *J. Chem. Phys.* **1971**, *54*, 3300–3306.

[118] Duschinsky, F. *Acta Physicochim. URSS* **1937**, *7*, 551–566.

[119] Manneback, C. *Physica* **1951**, *17*, 1001–1010.

[120] Sharp, T.; Rosenstock, H. *J. Chem. Phys.* **1964**, *41*, 3453–3463.

[121] Jankowiak, H.-C.; Stuber, J.; Berger, R. *J. Chem. Phys.* **2007**, *127*, 234101.

[122] Kubo, R. *Phys. Rev.* **1952**, *86*, 929.

[123] Schindler, M.; Kutzelnigg, W. *J. Chem. Phys.* **1982**, *76*, 1919–1933.

[124] Mebel, A. M.; Hayashi, M.; Liang, K. K.; Lin, S. H. *J. Phys. Chem. A* **1999**, *103*, 10674–10690.

[125] Niu, Y.; Peng, Q.; Deng, C.; Gao, X.; Shuai, Z. *J. Phys. Chem. A* **2010**, *114*, 7817–7831.

[126] Etinski, M.; Tatchen, J.; Marian, C. M. *J. Chem. Phys.* **2011**, *134*, 154105–154109.

[127] Bauer, V. J.; Clive, D. L.; Dolphin, D.; Paine III, J. B.; Harris, F. L.; King, M. M.; Loder, J.; Wang, S. W. C.; Woodward, R. B. *J. Am. Chem. Soc.* **1983**, *105*, 6429–6436.

[128] Richter, D. T.; Lash, T. D. *J. Org. Chem.* **2004**, *69*, 8842–8850.

[129] Shevchuk, S. V.; Davis, J. M.; Sessler, J. L. *Tetrahedron Lett.* **2001**, *42*, 2447–2450.

[130] Sessler, J. L.; Cyr, M.; Burrell, A. K. *Tetrahedron* **1992**, *48*, 9661–9672.

[131] Sessler, J. L.; Morishima, T.; Lynch, V. *Angew. Chem. Int. Ed.* **1991**, *30*, 977–980.

[132] Sessler, J. L.; Weghorn, S. J.; Hiseada, Y.; Lynch, V. *Chem. Eur. J.* **1995**, *1*, 56–67.

[133] Sessler, J. L.; Weghorn, S. J.; Morishima, T.; Rosingana, M.; Lynch, V.; Lee, V. *J. Am. Chem. Soc.* **1992**, *114*, 8306–8307.

[134] Vogel, E.; Köcher, M.; Schmickler, H.; Lex, J. *Angew. Chem. Int. Ed.* **1986**, *25*, 257–259.

[135] Ostapko, J.; Nawara, K.; Kijak, M.; Buczyńska, J.; Leśniewska, B.; Pietrzak, M.; Orzanowska, G.; Waluk, J. *Chem. Eur. J.* **2016**, *22*, 17311–17320.

[136] Sessler, J. L.; Brucker, E. A.; Weghorn, S. J.; Kisters, M.; Schäfer, M.; Lex, J.; Vogel, E. *Angew. Chem. Int. Ed.* **1994**, *33*, 2308–2312.

[137] Waluk, J.; Michl, J. *J. Org. Chem.* **1991**, *56*, 2729–2735.

[138] Benkyi, I.; Staszewska-Krajewska, O.; Gryko, D. T.; Jaszuński, M.; Stanger, A.; Sundholm, D. *J. Phys. Chem. A* **2020**, *124*, 695–703.

[139] Yoon, Z. S.; Cho, D.-G.; Kim, K. S.; Sessler, J. L.; Kim, D. *J. Am. Chem. Soc.* **2008**, *130*, 6930–6931.

[140] Yoon, M.-C.; Cho, S.; Suzuki, M.; Osuka, A.; Kim, D. *J. Am. Chem. Soc.* **2009**, *131*, 7360–7367.

[141] Cho, S.; Yoon, Z. S.; Kim, K. S.; Yoon, M.-C.; Cho, D.-G.; Sessler, J. L.; Kim, D. *J. Phys. Chem. Lett.* **2010**, *1*, 895–900.

[142] George, G. A.; Morris, G. C. *J. Mol. Spectrosc.* **1968**, *26*, 67–71.

[143] Ferguson, J.; Reeves, L. W.; Schneider, W. G. *Can. J. Chem.* **1957**, *35*, 1117–1136.

[144] Halasinski, T. M.; Hudgins, D. M.; Salama, F.; Allamandola, L. J.; Bally, T. *J. Phys. Chem. A* **2000**, *104*, 7484–7491.

[145] Briks, J. B. *Photophysics of Aromatic Molecules*; Wiley: New York, 1970.

[146] Halasinski, T. M.; Hudgins, D. M.; Salama, F.; Allamandola, L. J.; Bally, T. *J. Phys. Chem. A* **2000**, *104*, 7484–7491.

[147] Reddy, J. S.; Anand, V. G. *J. Am. Chem. Soc.* **2008**, *130*, 3718–3719.

[148] Shin, J.-Y.; Kim, K. S.; Yoon, M.-C.; Lim, J. M.; Yoon, Z. S.; Osuka, A.; Kim, D. *Chem. Soc. Rev.* **2010**, *39*, 2751–2767.

[149] Osuka, A.; Saito, S. *Chem. Commun.* **2011**, *47*, 4330–4339.

[150] Richert, C.; Wessels, J. M.; Mueller, M.; Kisters, M.; Benninghaus, T.; Goetz, A. E. *J. Med. Chem.* **1994**, *37*, 2797–2807.

[151] Stockert, J.; Cañete, M.; Juarranz, A.; Villanueva, A.; Horobin, R.; Borrell, J.; Teixidó, J.; Nonell, S. *Curr. Med. Chem.* **2007**, *14*, 997–1026.

[152] Oohora, K.; Kihira, Y.; Mizohata, E.; Inoue, T.; Hayashi, T. *J. Am. Chem. Soc.* **2013**, *135*, 17282–17285.

[153] Saeki, H.; Kurimoto, O.; Nakaoka, H.; Misaki, M.; Kuzuhara, D.; Yamada, H.; Ishida, K.; Ueda, Y. *J. Mater. Chem. C* **2014**, *2*, 5357–5364.